

Alma Mater Studiorum Università di Bologna
Archivio istituzionale della ricerca

Addressing the Elusive Polaronic Nature of Multiple Redox States in a π -Conjugated Ladder-Type Polymer

This is the final peer-reviewed author's accepted manuscript (postprint) of the following publication:

Published Version:

Fazzi D., Negri F. (2021). Addressing the Elusive Polaronic Nature of Multiple Redox States in a π -Conjugated Ladder-Type Polymer. ADVANCED ELECTRONIC MATERIALS, 7(1), 1-11 [10.1002/aelm.202000786].

Availability:

This version is available at: <https://hdl.handle.net/11585/818068> since: 2021-04-06

Published:

DOI: <http://doi.org/10.1002/aelm.202000786>

Terms of use:

Some rights reserved. The terms and conditions for the reuse of this version of the manuscript are specified in the publishing policy. For all terms of use and more information see the publisher's website.

This item was downloaded from IRIS Università di Bologna (<https://cris.unibo.it/>).
When citing, please refer to the published version.

(Article begins on next page)

This is the final peer-reviewed accepted manuscript of:

D. Fazzi, F. Negri, " Addressing the elusive polaronic nature of multiple redox states in a π -conjugated ladder-type polymer ", Adv. Elec. Mat. **7**, (2021), 2000786.

The final published version is available online at: [DOI:10.1002/aelm.202000786](https://doi.org/10.1002/aelm.202000786)

Rights / License:

The terms and conditions for the reuse of this version of the manuscript are specified in the publishing policy. For all terms of use and more information see the publisher's website.

Addressing the elusive polaronic nature of multiple redox states in a π -conjugated ladder-type polymer.

Daniele Fazzi,^{*1} Fabrizia Negri²

Dr. Daniele Fazzi

Institut für Physikalische Chemie, Department Chemie, Universität zu Köln, Luxemburger Str. 116 D-50939 Köln, Germany.

Prof. Fabrizia Negri

Università di Bologna, Dipartimento di Chimica ‘G. Ciamician’, Via F. Selmi, 2, 40126 Bologna, Italy.

E-mail: dfazzi@uni-koeln.de

Keywords: ladder type polymers, polarons, doping, radicaloids, redox species, broken-symmetry density functional theory

Abstract

Poly(benzimidazole-benzophenanthroline) (**BBL**) is a ladder-type conjugated polymer showing remarkable charge transport properties. Upon doping it displays various conductive regimes, leading to two *insulator-to-conductor* transitions. Such transitions have never been fully characterized, limiting our understanding about its charged states. Open issues are: (i) the electron/hole polaron relaxations, (ii) the structure-function relationships of multiple redox states and their connection with the conductive regimes, (iii) the role of protonation. Such knowledge-gaps are tackled *via* a comprehensive computational investigation of multiple redox species. Polarons show poly-radicaloid character, as revealed by combining broken-symmetry density functional theory, fragment orbital density and multi-reference analysis. Electron/hole polaron relaxations occur on the polymer chain, the former localizing on the benzophenanthroline moieties, while the latter on the benzimidazole units. Modelling of multiple charged species, up to one electron per repeat unit (1eru), reveals a complex *scenario* of *quasi*-degenerate states each featuring different spin multiplicity. Four redox states are responsible for the **BBL** *insulator-to-conductor* transitions. The two high conductive states refer to the electron polaron (0.25eru) and the redox species with 0.75eru. The insulating

regimes refer to the bipolaron (0.50eV) and the redox state with 1eV. Protonation is modelled, revealing polaron-like features in the spectroscopic properties.

1. Introduction

Ladder type conjugated polymers (LCPs) belong to the class of high-performance organic functional materials, featuring enhanced mechanical, thermal, chemical and opto-electronic properties with respect to their non-ladder systems.^[1] The unique functionalities of LCPs can be traced back to their molecular structure, which consists of double strand chains connected by condensed π -conjugated units, resulting in a periodic sequence of elements that resembles the shape of a ladder.^[2]

A consequence of such molecular architecture is the suppression of the dihedral angle linking two repeat units, thus leading to *quasi*-flat systems showing high long-range order at the molecular scale. In comparison to classical conjugated polymers, LCPs show a lower *intra*-chain torsional disorder, leading to a better π - π stacking and densely packed nano-structures.^[1a] Furthermore, planarity induces an extended π -electron delocalisation, providing small band- and optical-gap, and an overall low structural and electronic entropy.^[3]

Following such as simple as powerful structural design-rule a variety of LCPs were synthesised over the last decades. Examples dated back to 1960s are poly(benzimidazole-benzophenanthroline) (**BBL**)^[4] and its derivative **SBBL**, polyquinoxaline (**PQL**) and poly(phenoxazine) (**POL**).^[1a, 5] After these pioneering works, new LCPs belonging to the family of ladder type poly(p-phenylene) (**LPPPs**), poly(p-phenylene)s, poly(thioacenes), and D-A imide-derivatives, were recently proposed.^[6]

Despite their promising structure-property functions, LCPs have never overtook neither replaced traditional π -conjugated polymers as active materials for opto-electronic and energy saving applications. Reasons for that are related to issues encompassing (i) few effective synthetic strategies to construct defect free LCPs, (ii) poor solubility, (iii) complex

protonation states in aqueous media, and (iv) unclear redox mechanisms occurring both in solutions and solid state.

Amongst LCPs, **BBL** is the most investigated and promising one. It was synthesized in 1966 aiming at producing polymer fibres with high mechanical and thermal stability properties.^[4] Results were not promising and in 1982^[7] Kim renewed the attention on **BBL** suggesting it as a candidate for polymeric materials with high mechanical, thermal, chemical and electrical properties.^[8] Kim was amongst the first one documenting chemical doping in **BBL**, finding a remarkable enhancement in the electrical conductivity (σ) upon both oxidation and reduction. Both processes, increased σ of 12 orders of magnitude, from $10^{-12} \text{ Scm}^{-1}$ (pristine) to 2 Scm^{-1} (doped).^[8-9]

At the end of 1980s, Murray et al. explored the electrochemical doping of **BBL** in aqueous solutions and solid state films.^[10] Despite a broad set of techniques, e.g., CV, coulometry and spectro-electrochemistry, the complex redox behaviour of **BBL** remained largely unclear. Difficulties arose in understanding the following aspects: (i) the protonation state(s) and relative equilibrium in condensed phases, (ii) the redox processes which lead to multiple CV peaks and to two conductive states showing high and low σ values (a factor of ten between the two), (iii) the quantification of the amount of stored charge(s) per repeat units, and (iv) the spectroscopic and charge transport properties of multiple redox species.

At the end of 1990s Sandreczki et al.^[11] and Sariciftci et al.^[12] were able to perform electron spin resonance (ESR) and FT-IR spectro-electrochemistry experiments, getting insights into the multiple reduction processes of **BBL**. Contradicting conclusions however emerged, concerning the amount of consumed charge(s) per polymer unit during the doping processes, the assignments between the observed multiple redox states, and the two (high vs. low) electrical conductive states.^[13]

A plausible description was provided by Sariciftci et al. around 2000,^[14] by coupling CV, FT-IR and electrical conductivity measurements. In accordance to Murray et al.,^[13] they found that the electrical conductivity of **BBL** varied by changing the potential during electrochemical reduction, showing *two insulator-to-conductor* transitions, thus leading to two conductive states with high (*conductive state I*: $9 \times 10^3 \text{ Scm}^{-1}$ at -600mV in 0.1 M Bu_4NClO_4 -acetonitrile electrolyte), and two with low (*conductive state II*: $1.5 \times 10^3 \text{ Scm}^{-1}$ at -1000mV) conductivity. As inferred by Sariciftci et al.,^[14] the *two insulator-to-conductor* transitions referred to the presence of *four* reversible redox reactions (in contrast to Murray, who reported only two). Such redox species (named A, B, C, D) were assigned to two conductive and two insulating states, respectively. Sariciftci et al. proposed a multiple-charging reduction scheme in which the total number of consumed electron per repeat unit (eru) was measured as one, and the four redox species were classified as follow:^[14] A, eru = 0.25, *conductive state I*; B, eru = 0.50, *insulator state I*; C, eru = 0.85, *conductive state II*; D, eru = 1, *insulator state II*. FT-IR spectra showed induced absorption vibration (IRAV) bands tentatively assigned to different negatively charged species, however insights into the structural, vibrational and electronic properties of such hypothesized polaronic states were missing.

Despite such breakthrough in characterizing the complex redox behaviours of **BBL**, only phenomenological observations were reported, while fundamental understanding was lacking. Given such multifaceted electro-chemical and optical properties, **BBL** was broadly studied in the last two decades for different applications including pioneering works of Jenekhe et al.,^[15] on electron transport (n-type) organic field effect transistors ($\mu = 0.03 - 0.1 \text{ cm}^2\text{V}^{-1}\text{s}^{-1}$),^[16] heterojunction solar cells,^[17] thermoelectric devices,^[18] battery electrodes^[16c, 19] and bipolar high conductive D-A polymer interfaces.^[20]

For each application the role of multi redox states (involving either holes or electrons), and different protonated species (ubiquitously present in **BBL**, given its solubility in strong protonic acids) were never fully characterized nor understood.

Pioneering quantum-chemical calculations were reported in 1992 by Kim and Kertesz.^[21] They investigated the structural and electronic properties of neutral and protonated **BBL** within the framework of semi-empirical methods, however the approximated level of theory did not allow them neither to catch the underlying mechanisms, nor to explain the experimental data.

In 2016 Fabiano and Fazzi reported the first joint experimental and computational investigation about **BBL** thermoelectric and polaronic properties.^[18] Within the frame of density functional theory (DFT), they showed the presence of low-energy broken-symmetry unrestricted (BS-UDFT) solutions for a negatively charged state, leading to a spatially localized (electron) polaron over the ladder structure. In 2019, Zozoulenko et al.,^[22] reported DFT calculations for multiple charged states of **BBL**, up to two electrons per repeat unit (2 e^-). Despite Ref.^[22] represents an attempt in modelling multiple negatively charged states of **BBL**, it does not document the underlying DFT instabilities in determining the charged electronic wavefunctions, therefore the claimed state energies, spin and response properties should be revisited.

Recently, we extended the quantum-chemical investigation of single and double negatively charged states (electron polaron and bipolaron^[23]) of **BBL**.^[24] We confirmed that DFT leads to unstable solutions for the charged electronic wavefunction,^[25] given the multi-configurational character and electron correlation effects of charged states. We demonstrated how BS-UDFT might be an effective approach to overcome such issue, well describing the electron polaron/bipolaron localization in terms of spin densities and structural deformations,^[26] and providing a correct assessment of the vibrational and electron transport properties in comparison to experimental data.

Notably, even though **BBL** has been experimentally investigated over the last two decades, fundamental physico-chemical properties remain largely unsolved yet, limiting our basic understanding, therefore restricting potential improvements to the whole class of LCPs. In this work we aimed at filling this knowledge-gap by enlarging the quantum-chemical modelling of **BBL** to a broad set of multi-charged redox states. In particular, (i) we extended the investigation from electron to hole charged species, showing their different structural and spin relaxations over the polymer chain, together with their poly-radicaloid character. (ii) We modelled multi-negative charged states considering up to one electron per repeat unit (1eru), providing insights into the charging mechanisms and conductive species present upon doping. (iii) We predicted the structure-property relationships of protonated and protonated/reduced states, and ultimately, (iv) we calculated the response properties of all redox species so far considered, computing their vibrational and electronic spectra, and comparing the results with experimental data.

We were able for the first time to provide a solid understanding and interpretation to the experiments, by assigning the spectroscopic features of multiple redox species underlying the two observed *insulator-to-conductor* transitions,^[14] and by describing the role of protonated states in affecting the vibrational and electronic spectra of **BBL**. As such, the first high conductive state can be assigned to a polaron (0.25eru), while the first insulating state is attributed to a bipolaron (0.50eru). Two other states, bringing 0.75eru and 1eru, are related to the second conductive and insulating state, respectively. Protonated species show clear polaron-like features, detectable *via* IR and UV-Vis spectroscopies as suggested by our computational predictions.

Our study reconciles contradictory observations,^[10, 14, 22] addressing fundamental questions, namely: (i) what are the multiple-charging processes observed in **BBL** upon doping, (ii) how much charge is stored per polymer repeat unit, (iii) what are the polaronic species governing the high and low conductive states during the *insulator-to-conductor* transitions, (iv) how

electrons and holes relax over the polymer chain, and (ν) what are their main spectroscopic responses.

2. Results and Discussion

2.1 Electronic structure of BBL polarons and bipolarons: electron vs. hole.

Aiming at a full understanding of the charging processing occurring in **BBL** (see chemical structure and conformers in [Figure 1](#)), we modelled a variety of electronic states differing by the total charge (q) and spin state multiplicity. Charges were referred to be positive or negative, representing hole or electron doping, respectively. The electronic states for single ($|q| = 1e$) and double ($|q| = 2e$) charged species were named as: *polaron* - $q = \pm 1e$ (P^+ hole, P^- electron), state multiplicity doublet (D); *bipolaron* - $q = \pm 2e$ (B^+ , B^-), state multiplicities singlet (S) or triplet (T). Multiple redox species, in analogy to the experimental data,^[10, 14] were investigated only for the case of electrons, namely: $q = 3e^-$, state multiplicities doublet (D) or quartet (Q), and $q = 4e^-$, state multiplicities singlet (S), triplet (T), quintet (Qui), and $q = 5e^-$, state multiplicities Doublet (D), Quartet (Q) and Sextet (Sex) (see Supporting Information). For each electronic state, we optimized the structure and check the stability of the DFT wavefunction. If an instability was found, both electronic and nuclear coordinates were then re-optimized at the broken symmetry (BS) UDFT level, as already reported in Ref 18 and 24a for **BBL**. Generally, the basis of the BS formalisms and its broad application to inorganic, organic and hybrid compounds are specifically reported in Ref ^[24]. Further computational details are given in Supporting Information.

[Figure 1](#) reports the positive vs. negative polarons ($P^\pm(D)$ - red) and bipolarons ($B^\pm(S)$ - blue, $B^\pm(T)$ - black) stabilization energies (ΔE) for each **BBL** oligomer length (BBL1–8). ΔE is defined as the energy difference between the BS-UDFT and the standard DFT solutions. For $P^\pm(D)$ ΔE is computed as $\Delta E = E(\text{BS-UDFT}) - E(\text{UDFT})$, for $B^\pm(S)$ as $\Delta E = E(\text{BS-UDFT}) - E(\text{RDFT})$, and for $B^\pm(T)$ as the energy difference between triplet and singlet states, $\Delta E = E(T)$

- E(S). As already discussed in Ref.^[24a], electron polaron P-(D) shows an instability the longer is the **BBL** chain. Starting from BBL4, both *cis* and *trans* conformers show a BS-UDFT solution for P-(D), lower than the respective UDFT solution. For the case of bipolarons,^[24a] the situation is more pronounced than polarons. The instability of the DFT for a singlet bipolaron (B-(S)) is found starting from BBL2, leading to ΔE larger than 1 eV for long oligomers. The triplet bipolaron state (B-(T)) shows ΔE very much similar to the singlet B-(S), differing for less than 10^{-4} eV from the latter. The found BS solutions, recall for a multi-configurational character^[24b,c] and correlation effects of the electronic wavefunction^[27] for **BBL** polarons and bipolarons.

We extended the quantum-chemical investigation to positively charged states, namely hole polarons P+(D) and bipolarons B+(S), B+(T), as shown in [Figure 1](#). For P+(D) *cis* conformers do not show wavefunction instability, while *trans* do show BS solutions for certain lengths (BBL3, 5 and 7). As for electrons, hole singlet bipolaron states B+(S) report wavefunction instability, leading to ΔE larger than 1.5 eV for long oligomers. Contrary to electron bipolarons, hole B+(S) present a BS solution at the monomer level (BBL1) already, with $\Delta E = 0.5$ eV and 1 eV for *cis* and *trans*, respectively. This is a remarkable aspect, because it highlights the multi-reference (MR) and poly-radicaloid character^[28] of the double charged (bipolaron) hole-wavefunction.

In analogy to negatively charged species, the stabilization energies of hole bipolaron triplet states B+(T) are also reported in [Figure 1](#), following the same trend as discussed for B-(T). In general, the presence of low energy BS-UDFT solutions, regardless the nature of the charge, highlights a complex electronic structure *scenario* in which static electron correlation (SEC) and MR effects play relevant role.^[29] Despite BS-UDFT is based on a single-determinant approach,^[30] it has been demonstrated that it can qualitatively describe situations in which SEC^[24b-f,31] and MR or poly-radical characters are predominant,^[28,32] providing

reasonable results in comparison to MR methods.^[24b-f,33] Unquestionably, high-level quantum chemical methods, such as quantum Monte Carlo (QMC) techniques combined with the resonating-valence-bond (RVB) theory,^[34] would provide a better description of the electronic structure and correlation effects as compared to BS-UDFT or even wavefunction MR techniques, however such approaches are still too demanding to be applied for polymeric materials. A successful attempt was recently documented for the case of the neutral ground state of acenes, where MR effects were addressed *via* QMC/RVB,^[30] showing that the diradicaloid character is weaker as previously predicted *via* BS DFT, or wavefunction MR and coupled-clusters theories, though present.^[35]

To further stress the importance of electron correlation and MR effects in the description of multiple charged wavefunctions in ladder type systems, and to strengthen the BS-UDFT based approach, we performed a Fractional Occupation electron Density (FOD) analysis for some **BBL** oligomers in their neutral, polaron ($q=\pm 1e$) and bipolaron ($q=\pm 2e$) states. As introduced by Hansen et al.,^[36] FOD is a tool to gauge the MR character of a compound.^[37] FOD number (N_{FOD}) is a measure of how many highly correlated electrons are in the system. The larger is N_{FOD} the higher is the MR character of the system. As a consequence, in the context of HF or DFT approaches, the presence of BS solutions *might* appear.

[Table 1](#) collects the computed N_{FODs} for neutral, polaron and bipolaron states of few **BBL** oligomers. Notably, each electronic state shows high N_{FOD} values (≥ 0.7), which increase by lengthening the chain. The trend confirms a not negligible contribution from SEC in the description of the electronic wavefunction. The high N_{FODs} for the neutral state ([Table 1](#)) already indicate a pronounced poly-radical character of **BBL**.^[28] Accordingly, the analysis of the molecular orbitals (MOs) revealed an increase number of *quasi*-degenerate levels the longer is the oligomer chain, together with a high number of occupied MOs with fractional occupations between 0.3 and 1.98 (see Supporting Information).

Charged states, $P^\pm(S)$ and $B^\pm(D)$ show higher N_{FODs} than the neutral species, with values for holes larger than electrons. The FOD analysis justifies the presence of BS solutions,^[38] for **BBL** charged species ([Figure 1](#)), pointing out the role of SEC/MR effects in determining the electronic wavefunction of charged states.

To explicitly take into account MR effects and to prove their contributions in shaping the charged state electronic wavefunctions, we performed CASSCF/NEVPT2 calculations on a reference system, namely **BBL** monomer unit. Results are detailed in Supporting Information. Notably, CASSCF wavefunction for BBL1 $B^+(S)$ undoubtedly indicate a strong contribution of doubly excited determinants (i.e., $H,H \rightarrow L,L$ - with H the highest occupied molecular orbital and L lowest one) in the description of the ground state (~40%).

FOD and CASSCF/NEVPT2 calculations corroborate the BS-UDFT analysis for describing the multiple charged states of **BBL**, highlighting the importance of SEC effects in casting the electronic wavefunction of both electron and hole polarons and bipolarons. BS-UDFT solutions (*when found*) can represent an effective approximation to describe the complex MR/poly-radicaloid electronic structures of redox states in large conjugated systems. Such aspect is particularly valid for **BBL**, though we believe it is generally true for the whole class of LCPs.

To understand the relaxation and spatial confinements^[39] of electron vs. hole polarons and bipolarons along with the polymer ladder chain, we compared the computed spin densities in [Figure 2](#). A long oligomer, i.e., BBL5 as representative of the polymer, is considered. Both electron and hole polarons localize over a portion of the chain. Such aspect is a *physical property* of the system, the reason why can be traced back to the localized nature of the molecular orbitals as described at the DFT BS level.

While electron $P^-(D)$ localizes over the benzophenanthroline conjugated segment, hole $P^+(D)$ localizes over the benzimidazole moiety ([Figure 2](#)), leading to different structural and charge

relaxations. In particular, for P+(D) the spin density is localized around the imide units. Such different relaxations between electron and hole lead to different response properties, as discussed *infra*. Bipolaron states relax over two spatial separated chain segments, for both electrons and holes. The $B_{\pm}(S)$ spin densities reflect the radical character of bipolaron singlet state wavefunction. Bipolaron triplet states $B_{\pm}(T)$ relax over the same conjugated segments as $B_{\pm}(S)$ do.

The presence of heterogroups, such as carbonyls and imides, localize the *polaron defects*,^[40] favouring the confinement of the structural deformations and spin densities upon charging. We speculate that other LCPs might show BS DFT solutions for both neutral and charged states, therefore localized structural/spin density relaxations. We believe this is a general characteristic of LCPs, given their ladder structure and high π -electron delocalization, resulting in not negligible long-range electron correlations and MR/poly-radical effects.^[26b] However, the chain length at which the MR/poly-radical character become prominent has to be carefully evaluated for each polymer case, and moreover it should be benchmarked over a wide variety of methods.^[30]

2.2 Electronic structure of BBL multiple negatively charged states.

Multiple negatively charged species cover a crucial role in understanding the variety of redox and charge transport processes occurring in **BBL** upon charging,^[13-14, 20b, 41] as documented in the introduction. Upon reduction **BBL** shows two *insulator-to-conductor* transitions, having two conductive states (high, *conductive state I*: $9 \times 10^3 \text{ Scm}^{-1}$, and low, *conductive state II*: $1.5 \times 10^3 \text{ Scm}^{-1}$) and two insulating states. Sariciftci et al. tentatively assigned the multiple redox states to four species proposing the following multiple-charging reduction scheme:^[14]

- **BBL** (*pristine, insulator*) + qa = **BBL** ^{qa} (*species A, conductive state I*)
- **BBL** ^{qa} + qb = **BBL** ^{$(qa+qb)$} (*species B, insulating state I*)

- $\text{BBL}^{(qa+qb)} + q_c = \text{BBL}^{(qa+qb+qc)}$ (*species C, conductive state II*)
- $\text{BBL}^{(qa+qb+qc)} + q_d = \text{BBL}^{(qa+qb+qc+qd)}$ (*species D, insulating state II*)

The total consumed electron per repeat unit (eru) was measured as one ($q_a+q_b+q_c+q_d = 1\text{eru}$), and the partial charges transferred at different stages were determined as: $q_a=0.25\text{eru}$, $q_b=0.25\text{eru}$, $q_c=0.35\text{eru}$ and $q_d=0.15\text{eru}$. In such frame, the high *conductive state I* was referred to species A (0.25eru), while the low *conductive state II* as species C (0.85eru). The two insulating states were related to species B (0.50eru) and D (1eru), respectively.

To model such electron charging scheme, we considered the BBL4 oligomer, both *cis* and *trans* conformers, as a model system. In [Figure 3](#) are reported the energies of each multiple charged states (panel a) together with the relative spin densities (panel b). The correlation between the experimental redox species (A, B, C, D) and the charged states we modelled, is the following: species A corresponds to a total charge for BBL4 of $q = 1e^-$ (i.e., P-(D)) leading to 0.25eru, species B to $q = 2e^-$ (i.e., B-(S)/B-(T)) giving 0.50eru, species C to $q = 3e^-$ (state multiplicities D or Q) corresponding to 0.75eru, and species D to $q = 4e^-$ (state multiplicities Qui, T or S) with 1eru. We assumed that the experimental species C (measured as 0.85eru) can be approximated to the case of $q = 3e^-$, therefore 0.75eru.

BS solutions are indicated in [Figure 3](#), together with the state spin multiplicity. Notably, almost each state show a BS solution, remarking the role played by SEC and MR effects in governing the electronic wavefunction of such multiple negatively charged states. In BBL4 *cis*, upon charging the energies of all electronic states fall within the thermal activation energy at room temperature ($k_B T \sim 25 \text{ meV}$). For the case of bipolaron, singlet and triplet states, B-(S) and B-(T), are almost degenerate, leading to a $\Delta E(\text{S-T})$ very small ($|\Delta E| \sim 0.008 \text{ eV}$). The same holds for $q = 3e^-$ (i.e., 0.75eru), with doublet and quartet states degenerate, and for $q = 4e^-$ (1eru), with quintet, triplet and singlet states within $k_B T$. BBL4 *trans* slightly differs from *cis*, however all electronic negatively charged states reside below 0.08 eV of energy difference.

These findings highlight a remarkable aspect of **BBL**: multiple redox states show a variety of spin state multiplicities (e.g., singlet, doublet, triplet, quadruplet, quintet, etc.), and all states (for a given charge) reside within an energy difference of the order of $k_B T$ (or < 0.1 eV). Therefore, for a given redox species, multiple states with different spin multiplicities can become equally accessible and populated by thermal activation. The energetic *scenario* drawn in [Figure 3](#) underlies the complex and multifaceted redox behaviour of **BBL** upon electron doping.

The analysis of the spin densities, is reported in panel b, [Figure 3](#). Similarly to BBL5 ([Figure 2](#)), we can recognize that also for BBL4 electron P-(D) is mainly localized over a unit, and bipolarons B-(S) and B-(T) are localized over two. The cases of $q = 3e^-$ (0.75eru) and $4e^-$ (1eru) show localization over three and four units, respectively.

Given the low energy differences between states and the expected DFT energy error, we can **say** that states with the highest spin multiplicity *usually* feature the lowest energy. Notably, multiple charged states show a localized character, highlighting the polaronic nature of such redox species.

2.3 IR vibrational spectra of BBL polaron, bipolaron and multiple charged species.

Based on such model system, given the energies and spin multiplicities by checking the existence of BS-UDFT solutions, we were finally able to assign the redox species as those observed in the experiments by Murray et al.,^[10] and Sariciftci et al.,^[14] by computing the vibrational and electronic spectra.

In [Figure 4](#) are shown the computed IR spectra for each multiple (negative) charged states with respect to the experimental FT-IR spectro-electrochemical measurements from Ref.^[14].

The electron polaron P-(D) for both *cis* and *trans* conformers, shows four peculiar IRAV bands^[42] in the spectral regions 1650 cm^{-1} , 1500 cm^{-1} , 1280 cm^{-1} and 1200 cm^{-1} (labelled with * in [Figure 4](#), see Supporting Information for a spectroscopic assignment). The 1650 cm^{-1} band is associated with the anti-symmetric stretching mode of the two carbonyl groups

involved in the polaron structural relaxation (see spin density map, [Figure 3](#)). The intensity of such band is higher for the *cis* than the *trans*, given the different directionalities of the carbonyl groups. Another intense IR/V band is located around 1280-1300 cm⁻¹ being related to the CN stretching coupled with the CH rocking mode.

The computed IR spectra well reproduce the experimental one (despite the high signal-to-noise ratio of the latter),^[14] and allowed us to assign the high *conductive state I*, species A (0.25eru), to the electron polaron P-(D) state.

The IR spectra of bipolarons show a red shift of the 1650 cm⁻¹ band for both *cis* and *trans* conformers (toward 1635 cm⁻¹). Such band represents the anti-symmetric stretching of the carbonyl groups belonging to the two repeat units where the bipolaron is localized (see spin density map, [Figure 3](#)). To note, it is also the global intensification of all bands in the regions 1600 cm⁻¹, 1500 cm⁻¹ and 1300 cm⁻¹. For the case of **BBL** *trans* we can observe a gradual intensification of the band around 1350 cm⁻¹ (see [Figure 4](#)). Good agreement with the experimental data (see Supporting Information) is observed, allowing us to refer species B (0.50eru) i.e. the *insulator state*, as the electron bipolaron. Very little differences can be seen by comparing the computed IR spectra for singlet B-(S) and triplet B-(T) bipolarons (see Supporting Information).

Upon extra charging, towards $q = 3e^-$ and $4e^-$, with 0.75eru and 1eru respectively, the computed IR spectra change as follow: (i) a gradual red shift of the 1650 cm⁻¹ band toward 1600 cm⁻¹, and (ii) an intensification of the IR bands around 1500 cm⁻¹ and 1400-1350 cm⁻¹ regions. We can assign the calculated IR bands to the experimental ones observed for species C and D (see Supporting Information), therefore referring species C (*conductive state II*) to the charging case of $q = 3e^-$, and species D (*insulator state II*) to $q = 4e^-$. Differences between the computed IR spectra for each state spin multiplicity are very minors and reported in Supporting Information.

At the current stage it is difficult to discriminate between *cis* and *trans* conformers by comparing the calculated vs. experimental IR spectra. Experimentally samples are not pure *cis* or *trans* isomers, every chain containing a statistical distribution of both by virtue of the condensation polymerization method used.^[1b] Even though the detailed spectroscopic assignment will be the subject of another study, we can already observe some specific vibrational fingerprints.

For redox species A, the intense IR band at 1650 cm⁻¹ and the spectral shape around 1500 cm⁻¹ can be better assigned to conformer *cis*. For the redox species C (i) the sharp intense band around 1400 cm⁻¹ in the experimental data (here assigned to a quinoidal mode on a benzophenanthroline unit coupled with the CN stretching) can be attributed to the *trans* conformer, and (ii) the two intense experimental bands around 1500 cm⁻¹ region can be interpreted as a superposition of bands belonging to both *cis* and *trans*. For redox species D, we can recognize the IR bands at 1600 cm⁻¹ for both **BBL** *cis* and *trans*, together with the intense band at 1350 cm⁻¹.

The good correlation between the theoretical and experimental data directly validates our BS DFT approach in describing the electronic structure and response properties of multiple charged states in LCPs.^[24] Moreover, we were able to assign for the first time all redox species (A, B, C, D) as previously identified experimentally,^[14] however never characterized. Summarizing, we can refer the high *conductive state I* (species A) to the electron P-(D) doublet state, and the low *conductive state II* (species C) to the case with a total charge $q = 3e^-$ for BBL4, i.e., 0.75eru, being either a doublet or a quartet electronic state ([Figure 3](#)). The two *insulating states* can be assigned to bipolarons (either B-(S) or B-(T)), and to a state with a total charge $q = 4e^-$ for BBL4 (i.e., 1eru) showing either quintet, triplet or singlet state multiplicity ([Figure 3](#)).

Given the current experimental data-set available in literature,^[14] it is difficult to discriminate amongst different **BBL** conformers and state multiplicities playing during the multi-electron

doping processes. Further experimental data, such as electron spin resonance spectroscopy, would be required.

2.4 Electronic spectra of BBL polaron, bipolaron and multiple charged species.

A possible way to get insights into the nature of multiple redox states upon electron doping, can be by analysing the electronic transitions of charged species.

In [Figure 5](#) is reported the comparison between the computed vertical electronic transitions, for each multiple charged state, between **BBL** *cis* and *trans*. It can be noted that the comparison **BBL** *cis* vs. *trans* leads to markedly different electronic spectroscopic responses. The excitation energies of **BBL** *trans* for the polaron ($q = 1e^-$), bipolaron ($q = 2e^-$), $q = 3e^-$ and $q = 4e^-$ are generally lower in energy, showing broader spectra, than the *cis*. The negatively charged species of **BBL** *trans* show dipole active excited states in the mid-IR region, while for **BBL** *cis* such low-energy excited states, though present, are optically forbidden (or with negligible oscillator strength, see Supporting Information).

While polaron and bipolaron show similar electronic transitions, within each conformer, the case for $q = 3e^-$ (0.75eru) and $4e^-$ (1eru) differ, leading to more intense oscillator strengths and broader absorption bands.

Spectro-electrochemical data reported by Murray et al.,^[10] and recent UV-Vis spectra recorded upon electron chemical doping,^[18, 20b] well match the theoretical predictions of the excited state for the P-(D) species. In Ref^[10] are reported also the UV-Vis spectra by changing the reduction potential. Evidences of an enhancement in the band intensities around 2.5-2.3 eV, and further below at 1.3 eV, well match the computed electronic spectra for **BBL** *trans*, [Figure 5](#). The published data document the presence of an absorption band starting at 900 nm (1.3 eV), which increases its intensity by increasing the redox potential. For the case of **BBL** *trans*, we indeed predicted low-lying excited states ($< 1eV$) for both electron polarons and bipolarons.

As reported before for the IR spectra, the active species present in solution or in thin films are most likely a mixture of **BBL** *cis* and *trans* conformers.

Regardless specific assignments, given the differences in the computed electronic transitions for multiple redox states, we envisage that UV-Vis spectro-electrochemistry – around 2-1.5 eV and down to 1.3-0.3 eV spectral regions – can be a valuable tool to discriminate amongst **BBL** conformers *and* between different electronic redox states playing upon electron charging, as clearly shown in [Figure 5](#).

2.5 Role of protonation in **BBL** neutral and charged species.

A relevant question still has to be answered in literature regards the effects of protonation, and the mutual presence of protonated and reduced states as induced by doping, in affecting **BBL** structural and spectroscopic properties.^[8, 10] This aspect is very relevant in the literature of **BBL** and other LCPs, being such polymers processed by using strong protonic acids to favour their solubility and processability. As a consequence, a fraction of protonated species is inevitably present in the active material, eventually affecting the opto-electronic properties.

[Figure 6](#) compares the computed IR and UV-Vis spectra for the following three cases of **BBL4 cis**: a protonated oligomer (1H⁺ per repeat unit, named 4H⁺), a charged oligomer with $q = 4e^-$ (1eru) and a protonated/charged oligomer (4H⁺/4e⁻). The protonated species shows an intense IR band at 1000 cm⁻¹ (see * [Figure 6](#)). Such transition, associated to the CH rocking coupled with the NH rocking localised on one benzophenanthroline unit, is always present in any IR spectrum of *pristine* **BBL**, as published so far.^[8, 14] On the contrary, as evident from our calculations, such band is *not* related to a pristine species, rather to a (partially) protonated species. The computed IR spectra of neutral **BBL cis** and *trans* (see [Figure 4](#)) in fact do not show any intense IR band around 1000 cm⁻¹.

Notably, the intensity of the IR band associated to the protonated species is orders of magnitude higher than the band intensities of the neutral species in the same spectral region.

We speculated that even low concentrations of protonated species in *pristine* samples can lead

to an intense IR band at 1000 cm^{-1} (as reported in Ref.^[8, 14]). To note, it is also the broadening of the IR spectrum of BBL4 protonated species (4H^+) in the region of the carbonyl bands (see * at 1700 cm^{-1} in [Figure 6](#)), shifting the frequencies towards high wavenumbers. Such spectral spread was already reported in early experimental data by Kim,^[8] however never carefully investigated. We can prove that the broadening at 1700 cm^{-1} is due to the presence of a protonated species (see Supporting Information).

In [Figure 6](#) are shown also the computed electronic transitions (TDDFT data) for the protonated (4H^+), charged ($q = 4e^-$, $1e^+$) and protonated/charged ($4\text{H}^+/4e^-$) species. The protonated (4H^+) species shows a distinctive absorption band around 1.2 eV , leading to a spectrum remarkably different than the charged or protonated/charged species. Such low-energy band is the $S_0 \rightarrow S_1$ transition, described (see Supporting Information) as single excitations from singly occupied to unoccupied orbitals localized over few units.

Unfortunately, we could not find experimental data to corroborate our calculations. We otherwise believe our theoretical spectroscopic predictions may serve as a valuable tool for both theoreticians and experimentalists to characterize the multiple redox *and* protonated species of **BBL**, present in solution or solid state.^[10] Spin densities for each protonated and charged case are reported as insets in [Figure 6](#) too, showing the localization of the spins, therefore the polaronic nature of such multiple redox/protonated species.

3. Conclusion

LCPs gained a renewed interest owing to their remarkable chemical, mechanical, optoelectronic, and energy-conversion properties. Amongst LCPs, **BBL** is the most investigated one, showing the highest electron mobility ($0.1\text{ cm}^2/\text{Vs}$), electrical conductivity (1.7 Scm^{-1}) and thermo-electric power factor ($0.43\text{ }\mu\text{Wm}^{-1}\text{K}^{-2}$). Such outstanding figures-of-merit are achieved *via* (electro)-chemical doping, leading to a series of multiple redox states whose structural, electronic and optical responses have never been comprehensively rationalised.

Despite the numerous reports on **BBL**, the understanding of fundamental electronic and chemical-physical properties remains poor. We filled such knowledge-gap through an extended quantum-chemical investigation modelling the multiple charged states of **BBL**, assessing their structural, spin and spectroscopic properties.

We found that the electronic wavefunction of charged states (e.g., polarons, bipolarons, and multiple redox states) shows remarkable electron correlation effects and multi-configurational characters, features that we addressed *via* a combined use of BS-UDFT and FOD calculations, as well supported by multi-reference (MR) wavefunction methods.

Holes (i.e., oxidised species) showed higher MR/radicaloid character than electrons (reduced species). MR wavefunction calculations corroborated such aspect, reporting a strong contribution of double excitations in the description of the **BBL** ground state hole bipolaron wavefunction.

Comparing the electron and hole states, we found that the structural and spin-density relaxations of polaron, bipolaron and multiple redox states showed distinctive differences.

Electrons relax upon the benzophenanthroline segments, while holes localize over the benzimidazole moieties. Both polarons are spatially localized, allowing **BBL** to host multiple charges, a property that can be exploited for thermo-electric and electrode-battery applications.

Upon electro-chemical doping **BBL** shows multiple conductive regimes, leading to two *insulator-to-conductor* transitions, as reported in literature. We modelled such complex redox *scenario* by mimicking the multiple charged states of **BBL** up to 1eru. We found a variety of spin state multiplicities (e.g., singlet, doublet, triplet, quartet, quintet, etc.) by varying the charge accommodated on the chain, revealing a wide range of *quasi*-degenerate electronic states all lying within $k_B T$, or below 0.1 eV. Notably, given a certain charge, states with different spin multiplicities can be thermally populated.

The multiple redox states can be represented as follow: the polaron as 0.25eru ($q=1e^-$), the bipolaron as 0.50eru ($q=2e^-$), and the multiple redox states as 0.75eru ($q=3e^-$) and 1eru ($q=4e^-$).

We were able to assign the conductive/insulating regimes observed in literature to specific multiple charged states of **BBL**, by comparing the computed IR vibrational spectra to the experimental ones. We found that the high *conductive state I* can be related to the polaron (doublet), the low *conductive state II* to the redox species with 0.75eru (being either doublet or quartet), the two *insulating states* to the bipolaron (either singlet or triplet), and to the redox case with 1eru (either quintet, triplet or singlet).

Furthermore, we assigned the main intense IR/V bands of the polaronic species to the anti-symmetric stretching of the carbonyl groups (1650 cm^{-1}), and to the quinoidal mode localized over the benzophenanthroline units and coupled with the imide moieties. A blue shift of the 1650 cm^{-1} band is predicted, by moving from polaron (0.25eru), to bipolaron (0.50eru) and up to 1eru charged state. This clear assignment would allow future experimental and quantitative monitoring of the doping levels and conductive species upon doping.

We evaluated the electronic transitions of multiple redox states, finding that **BBL** *cis* and *trans* conformers show remarkable variations in the excited states. The latter shows low-energy optical allowed transitions, otherwise not active in the *cis*.

Finally, we addressed the role of protonation in **BBL**. Protons, localized on the imide units, induce a polaron-like spin density. A peculiar vibrational signature of protonated species is the intense IR band at 1000 cm^{-1} . Moreover, protonated species shows a distinctive electronic absorption band, leading to an absorption spectrum remarkably different than the charged or protonated/charged cases.

Our theoretical predictions and computed vibrational and electron spectra of multiple charged **BBL** species may serve as valuable tools for both theoreticians and experimentalists to further characterize the complex redox and protonation behaviour of **BBL** (and other LCPs), both in solution and solid state. Our study finally reconciles contradictory experimental and computational observations, shedding light onto the structure-property functions of **BBL**, so far the most prominent polymer amongst LCPs.

4. Experimental Section/Methods

Detailed information concerning each aspect of the quantum-chemical calculations are reported in Supporting Information.

Supporting Information

Supporting Information is available from the Wiley Online Library or from the author.

Conflict of Interest

The authors declare no conflict of interest.

Acknowledgements

D.F. acknowledges the Deutsche Forschungsgemeinschaft (DFG) for a grant (FA 1502/1-1 “Molecular Understanding of Thermo-Electric Properties in Organic Polymers”) and the Regional Computing Centre (RRZK) of Universitaet zu Koeln, for providing computing time and resources on the HPC RRZK CHEOPS. F. N. acknowledges the financial support of University of Bologna (RFO).

Received: ((will be filled in by the editorial staff))

Revised: ((will be filled in by the editorial staff))

Published online: ((will be filled in by the editorial staff))

Figure 1. Top panel, chemical structures of *cis* and *trans* BBL conformers. Bottom panels: stabilization energy ΔE (see definition in the main text) for polaron doublet P(D) (red), bipolaron singlet B(S) (blue) and triplet B(T) (black) states by changing the oligomer size n (n = #number of unit, 1-8), for electron (left) and hole (right). DFT functional: ω B97X-D, basis set: 6-31G*. Negative energies refer to BS-UDFT calculations ($P^\pm(D)$, $B^\pm(S)$), or UDFT calculations ($B^\pm(T)$). Reproduced with permission.^[24] Copyright 2019, RSC. Data for electrons are readapted from Ref^[24].

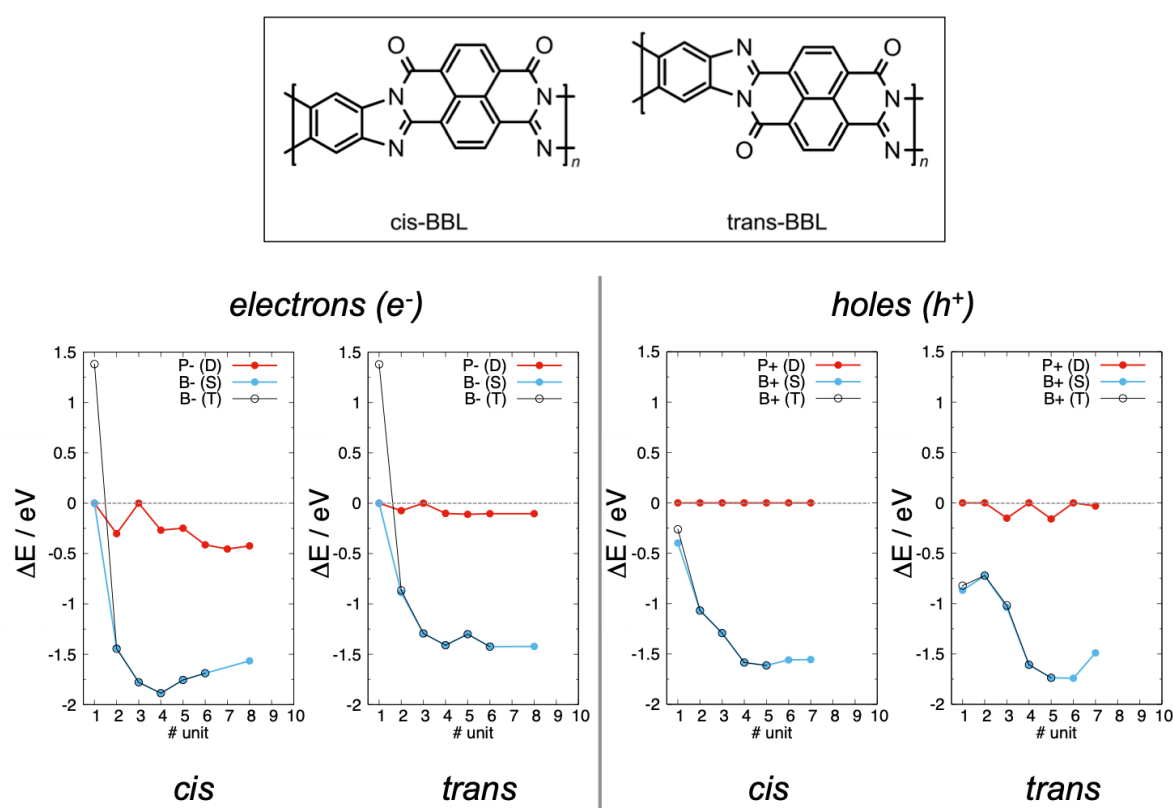


Figure 2. Electrons (top) and holes (bottom) spin densities (ρ) calculated at the BS-UDFT level of theory (ω B97X-D/6-31G*), for polarons doublet (P(D)), bipolaron singlet (B(S)), and UDFT for bipolaron triplet (B(T)) states. Spin densities were calculated as $\rho \square \square \rho \square \square \rho \square \square$ at isovalues of 0.001 \AA^3 \square Data refer to BBL5 *trans*.

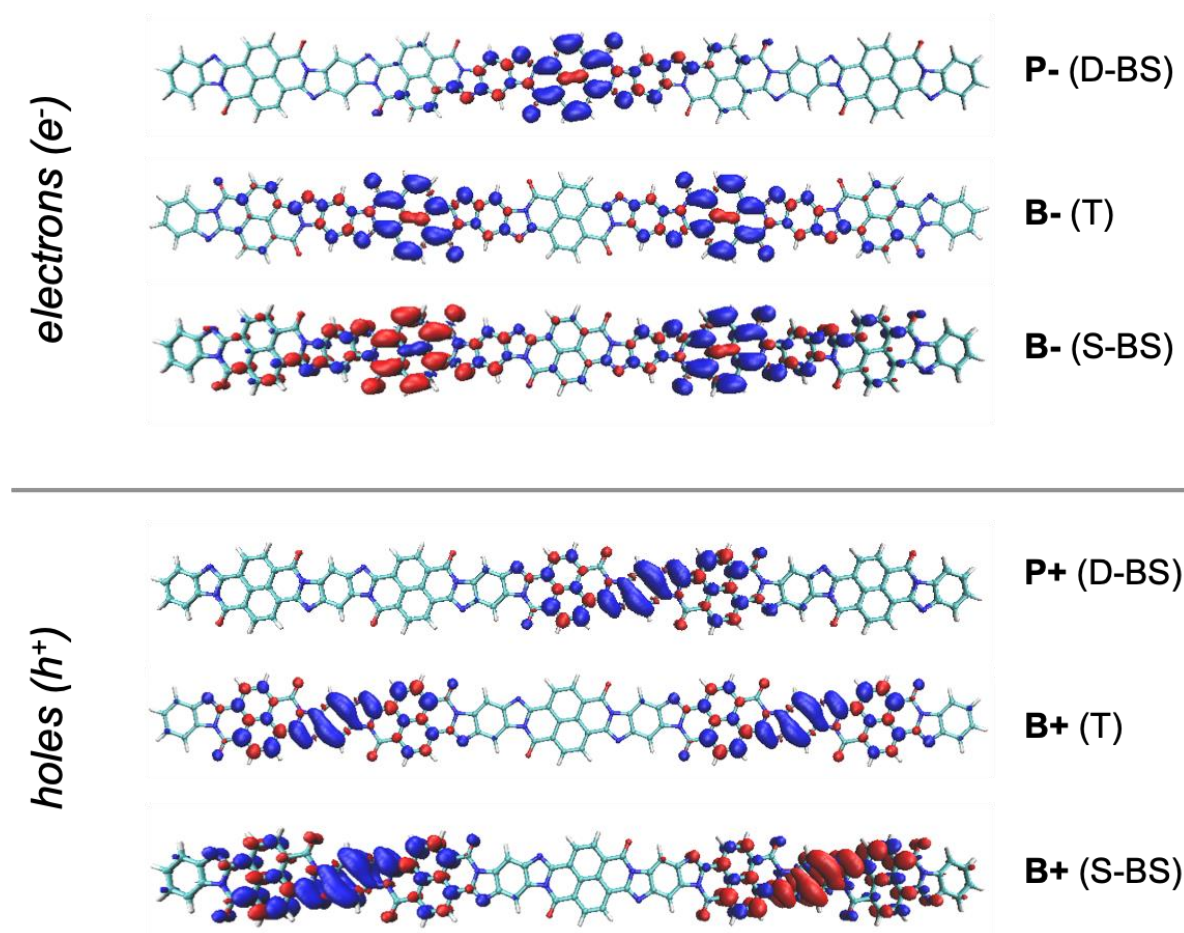


Figure 3. Top panels: calculated energy difference for electronic negatively charged states, as defined by the total charge q . Polaron, $q=1e^-$, doublet (D). Bipolaron, $q=2e^-$, singlet (S) or triplet (T). $q=3e^-$, doublet (D) or quadruplet (Q). $q=4e^-$, quintet (Qui), triplet (T) or singlet (S). Broken-symmetry (BS) solutions are indicated, when found. Total negative charges per BBL4, correspond to eru, namely: $q=1e^-$ (0.25eru), $q=2e^-$ (0.50eru), $q=3e^-$ (0.75eru) and $q=4e^-$ (1eru). Both *cis* (left) and *trans* (right) conformers are reported. Bottom panel: computed spin densities for each negative charged state. Level of theory (ω B97X-D/6-31G*).

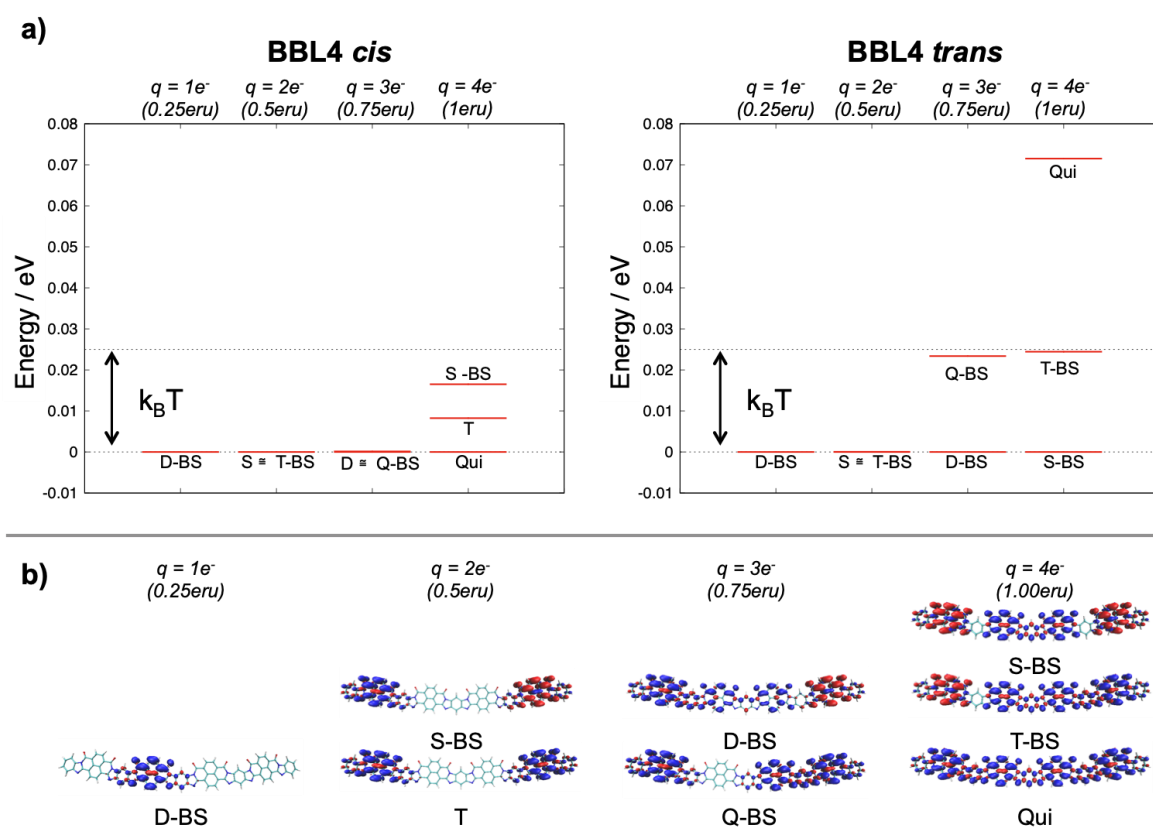


Figure 4. Top panel, theoretical IR spectra for BBL4 *cis* (left) and *trans* (right) computed for neutral (green line) and different negative charged states, namely: $q=1e^-$ (0.25eru) species A, $q=2e^-$ (0.50eru) species B, $q=3e^-$ (0.75eru) species C, and $q=4e^-$ (1eru) species D. Labels * mark relevant IRAV modes. Computed frequencies (ω B97X-D/6-31G*) were rescaled by a scaling factor 0.93 to match experimental data. Bottom panel: experimental FT-IR spectro-electrochemistry data, Reproduced and readapted with permission.^[14] Copyright 2019, ACS. Redox species A (0.25eru), B (0.50eru), C (0.85eru) and D (1eru).

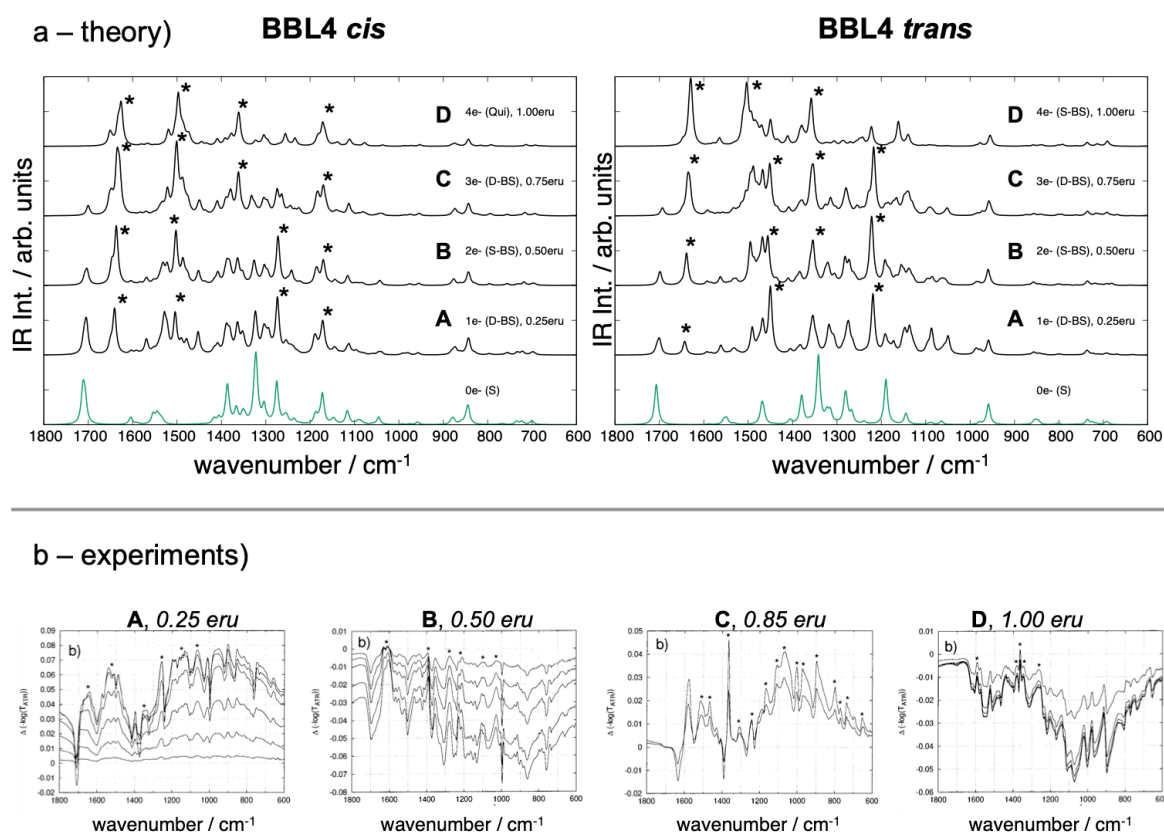


Figure 5. Computed electronic vertical transition energies (unscaled values) at the time-dependent TD-DFT (ω B97X-D/6-31G*) for electron polaron (P(D)), bipolaron (B(S), B(T)), $q=3e^-$ (doublet, D) and $q=4e^-$ (quintet or singlet) states. BBL4 *cis* (left) and *trans* (right) conformers are reported. Spectra were obtained as convolution of Lorentzian functions.

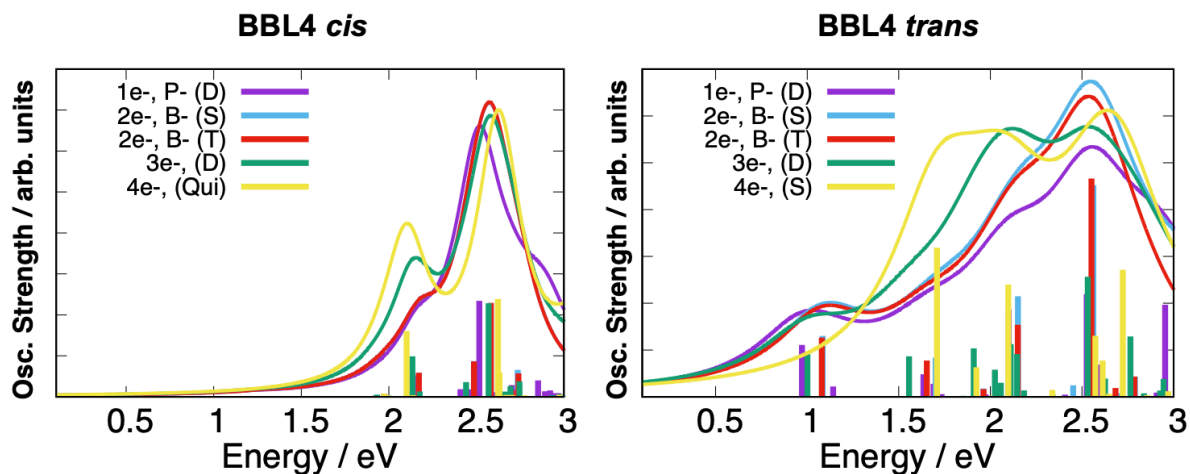


Figure 6. Left panel, computed IR spectra (scaling factor 0.93) for BBL4 *cis* protonated ($4H^+$), charged ($q = 4e^-$, 1eru) and protonated/charged ($4H^+/4e^-$) species (all quintet state multiplicity), together with the spin densities. Right panel, relative computed TD-DFT vertical transition energies (unscaled values).

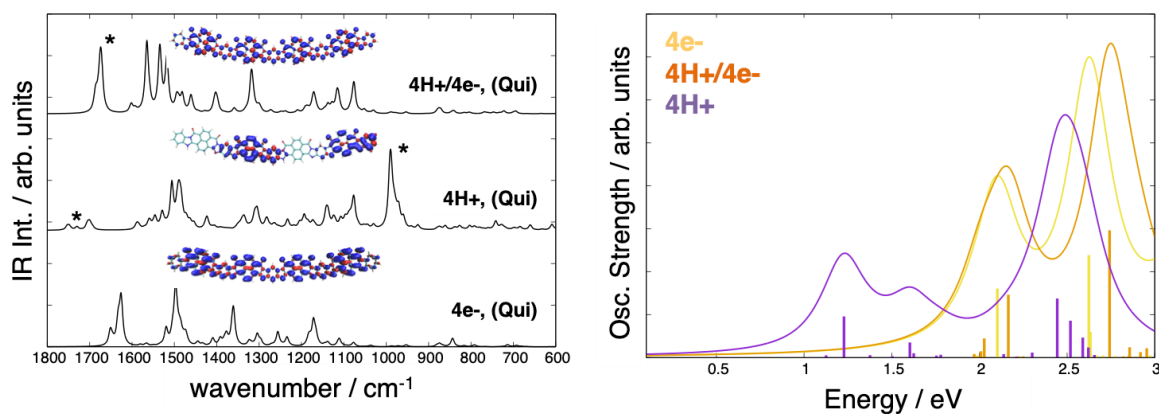


Table 1. FOD numbers (N_{FOD}) of neutral, electron/hole polarons ($P^{\pm}(\text{D})$) and bipolarons $B^{\pm}(\text{S})$ **BBL** *cis* and *trans* oligomers ($n=1,4$). A label (*) identified those species where a BS-UDFT solution was found.

		N_{FOD}				
BBLN		N (S)	P+ (D)	P- (D)	B+ (S)	B- (S)
1	<i>cis</i>	0.6835	1.507	0.768	2.153*	0.867
	<i>trans</i>	0.6628	1.630	0.763	2.483*	0.869
2	<i>cis</i>	1.339	2.275	1.879*	3.136*	2.389*
	<i>trans</i>	1.307	2.235	1.749*	3.284*	2.170*
3	<i>cis</i>	1.993	2.970	2.631	3.869*	3.213*
	<i>trans</i>	1.950	2.900*	2.509	3.804*	3.053*
4	<i>cis</i>	2.640	3.622	3.329*	4.538*	4.029*
	<i>trans</i>	2.593	3.547	3.206*	4.470*	3.808*

References

- [1] a) J. Lee, A. J. Kalin, T. Yuan, M. Al-Hashimi, L. Fang, *Chem. Sci.* **2017**, *8*, 2503; b) U. Scherf, *J. Mater. Chem.* **1999**, *9*, 1853; c) R. S. Sprick, A. Thomas, U. Scherf, *Polym. Chem.* **2010**, *1*, 283; d) E. Khodabakhshi, C. Ramanan, J. J. Michels, S. Bonus, D. Hertel, K. Meerholz, M. Forster, U. Scherf, P. W. M. Blom, *Adv. Elec. Mater.* **2020**, *6*, 2000082; e) R. Lu, Y. Han, W. Zhang, X. Zhu, Z. Fei, T. Hodsdon, T. D. Anthopoulos, M. Heeney, *J. Mater. Chem. C* **2018**, *6*, 2004; f) I. Belaish, D. Davidov, H. Selig, M. R. McLean, L. R. Dalton, *Adv. Mater.* **1989**, *11*, 387; g) W. Graupner, J. Partee, J. Shinar, G. Leising, U. Scherf, *Phys. Rev. Lett.* **1996**, *77*, 2033.
- [2] A.-D. Schlüter, *Adv. Mater.* **1991**, *3*, 282.
- [3] Y. Yin, S. Zhang, D. Chen, F. Guo, G. Yu, L. Zhao, Y. Zhang, *Polym. Chem.* **2018**, *9*, 2227.
- [4] R. L. V. Deussen, *Polym. Lett.* **1966**, *4*, 211.
- [5] L. Yu, M. Chen, L. R. Dalton, *Chem. Mater.* **1990**, *2*, 6, 649.
- [6] a) A. Vogel, M. Forster, L. Wilbraham, C. L. Smith, A. J. Cowan, M. A. Zwiijnenburg, R. S. Sprick, A. I. Cooper, *Faraday Discuss.* **2019**, *215*, 84; b) J. Lee, B. B. Rajeeva, T. Yuan, Z. H. Guo, Y. H. Lin, M. Al-Hashimi, Y. Zheng, L. Fang, *Chem. Sci.* **2016**, *7*, 881; c) Y. Chen, H. Li, M. Tang, S. Zhuo, Y. Wu, E. Wang, S. Wang, C. Wang, W. Hu, *J. Mater. Chem. A* **2019**, *7*, 20891.
- [7] H. Siihira, E. J. Louis, A. G. MacDiarmid, C. K. Chiang, A. J. Heeger, *J. Chem. Soc., Chem. Commun.* **1977**, 578-580.
- [8] O.-K. Kim, *Journal of Polymer Science: Polymer Letters Edition* **1982**, *20*, 663.
- [9] O.-K. Kim, *Molecular Crystals and Liquid Crystals* **1984**, *105:1*, 161.
- [10] K. Wilbourn, R. W. Murray, *Macromolecules* **1988**, *21*, 89.
- [11] T. Zheng, F. Badrun, I.M. Brown, D.J. Leopold, T.C. Sandreczki, *Synthetic Metals* **1999**, *107*, 39.
- [12] T. Yohannes, H. Neugebauer, S. Luzzati, M. Catellani, S. Yi., S. A. Jenekhe, N. S. Sariciftci, *Synthetic Metals* **2001**, *119*, 319.
- [13] K. Wilbourn, R. W. Murray, *J. Phys. Chem.* **1988**, *92*, 3642.
- [14] T. Yohannes, H. Neugebauer, S. Luzzati, M. Catellani, S. A. Jenekhe, N. S. Sariciftci, *J. Phys. Chem. B* **2000**, *104*, 9430.
- [15] a) H. Antoniadis, M. A. Abkowitz, J. A. Osaheni, S. A. Jenekhe, M. Stolka, *Chem. Mat.* **1994**, *6*, *1*, 63; b) M. M. Alam, S. A. Jenekhe, *J. Phys. Chem. B* **2002**, *106*, 11172.
- [16] a) A. Babel., S. A. Jenekhe, *J. Am. Chem. Soc.* **2003**, *125*, 13656; b) A. L. Briseno, F. S. Kim, A. Babel, Y. Xia, S. A. Jenekhe, *J. Mater. Chem.* **2011**, *21*, 16461; c) H. Sun, J. Gerasimov, M. Berggren, S. Fabiano, *J. Mater. Chem. C* **2018**, *6*, 11778.
- [17] S. A. Jenekhe, S. Yi, *App. Phys. Lett.* **2000**, *77*, 2635.
- [18] S. Wang, H. Sun, U. Ail, M. Vagin, P. O. Persson, J. W. Andreasen, W. Thiel, M. Berggren, X. Crispin, D. Fazzi, S. Fabiano, *Adv. Mater.* **2016**, *28*, 10764.
- [19] a) J. Wu, X. Rui, C. Wang, W.-B. Pei, R. Lau, Q. Yan, Q. Zhang, *Adv. Ener. Mater.* **2015**, *5*, 1402189; b) J. Xie, W. Chen, Z. Wang, K. C. W. Jie, M. Liu, Q. Zhang, *Chem. Asian J.* **2017**, *12*, 868.
- [20] a) X. L. Chen, S. A. Jenekhe, *Macromolecules* **1997**, *30*, 1728; b) K. Xu, H. Sun, T.-P. Ruoko, G. Wang, R. Kroon, N. B. Kolhe, Y. Puttisong, X. Liu, D. Fazzi, K. Shibata, C.-Y. Yang, N. Sun, G. Persson, A. B. Yankovich, E. Olsson, H. Yoshida, W. M. Chen, M. Fahlman, M. Kemerink, S. A. Jenekhe, C. Müller, M. Berggren, S. Fabiano, *Nat. Mater.* **2020**, *19*, 738.
- [21] S. Y. Hong, M. Kertesz, Y. S. Lee, O.-K. Kim, *Macromolecules* **1992**, *25*, 5424.
- [22] S. Ghosh, V. Gueskine, M. Berggren, I. V. Zozoulenko, *J. Phys. Chem. C* **2019**, *123*, 15467.

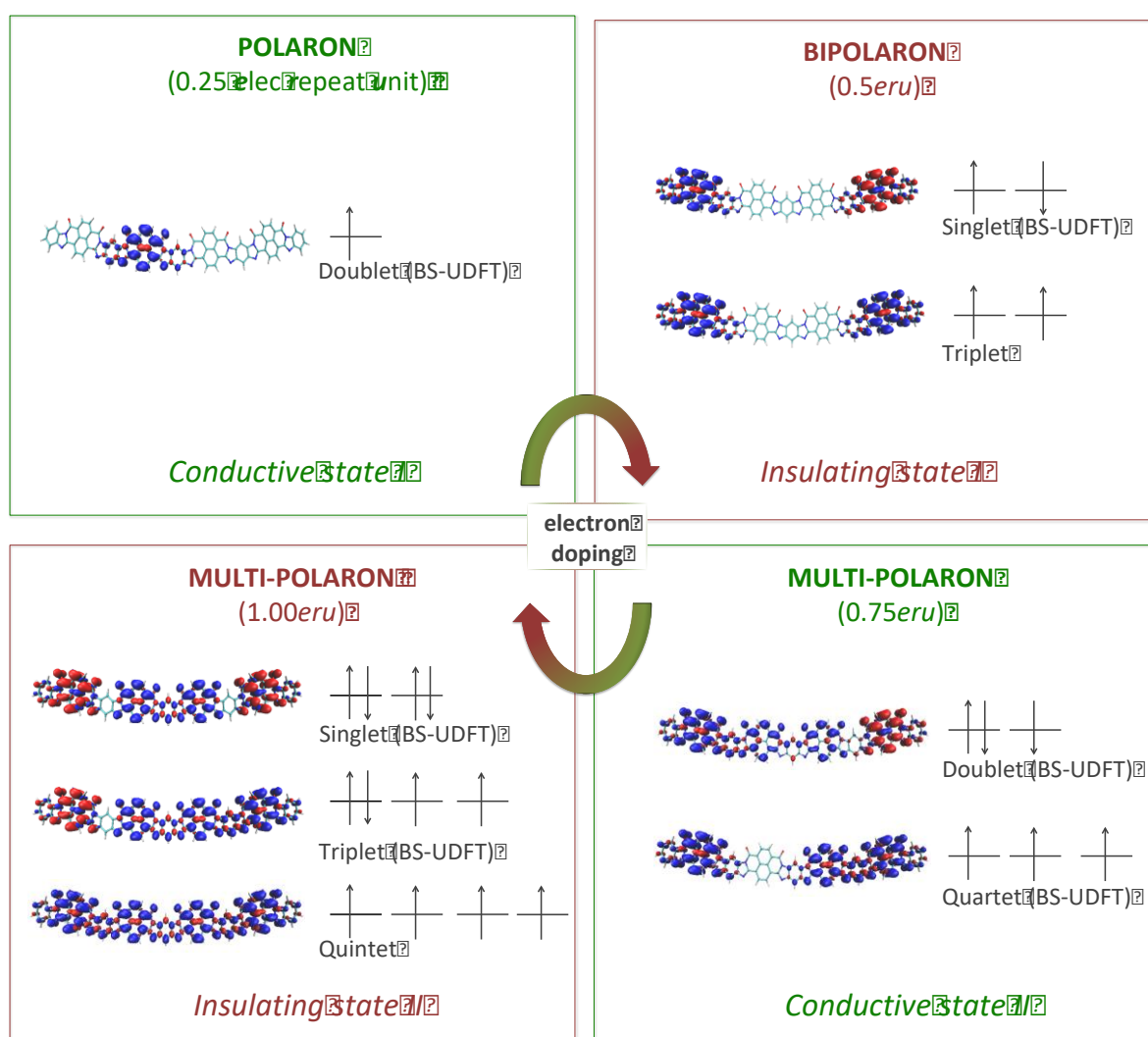
- [23] a) I. Zozoulenko, A. Singh, S. K. Singh, V. Gueskine, X. Crispin, M. Berggren, *ACS Appl. Polym. Mater.* **2019**, *1*, 1, 83; b) J. L. Brédas, G. B. Street, *Acc. Chem. Res.* **1985**, *18*, 309; c) J. Li, G. D'Avino, A. Pershin, D. Jacquemin, I. Duchemin, D. Beljonne, X. Blase, *Phys. Rev. Mater.* **2017**, *1*, 025602.
- [24] a) D. Fazzi, S. Fabiano, T.-P. Ruoko, K. Meerholz, F. Negri, *J. Mater. Chem. C* **2019**, *7*, 12876. b) P. M. Lahti, A. S. Ichimura, J. A. Sanborn, *J. Phys. Chem. A* **2001**, *105*, 251-260. c) V. Bachler, G. Olbrich, F. Neese, K. Wieghardt, *Inorg. Chem.*, **2002**, *41*, 4179-4193. d) Noodleman, L. *J. Chem. Phys.* **1981**, *74*, 5737. e) Noodleman, L.; Davidson, E. R. *Chem. Phys.* **1986**, *109*, 131. f) Ovchinnikov, A. A.; Labanowski, J. K. *Phys. Rev. A* **1996**, *53*, 3946. g) Adamo, C.; Barone, V.; Bencini, A.; Totti, F.; Ciofini, I. *Inorg. Chem.* **1999**, *38*, 1996.
- [25] J. P. Perdew, A. Savin, K. Burke, *Phys. Rev. A* **1995**, *51*, 4531.
- [26] a) S. Wang, D. Fazzi, Y. Puttisong, M. J. Jafari, Z. Chen, T. Ederth, J. W. Andreasen, W. M. Chen, A. Facchetti, S. Fabiano, *Chem. Mat.* **2019**, *31*, 3395; b) M. Bendikov, H. M. Duong, K. Starkey, K. N. Houk, E. A. Carter, F. Wudl, *J. Am. Chem. Soc.* **2004**, *126*, 7416.
- [27] S. Yamanaka, T. Kawakami, H. Nagao, K. Yamaguchi, *Chem. Phys. Lett.* **1994**, *231*, 25.
- [28] G. Salvitti, F. Negri, A. J. Perez-Jimenez, E. San-Fabian, D. Casanova, J. C. Sancho-Garcia, *J. Phys. Chem. A* **2020**, *124*, 3590.
- [29] a) J. L. Bao, L. Gagliardi, D. G. Truhlar, *J. Phys. Chem. Lett.* **2018**, *9*, 2353; b) C. M. Marian, A. Heil, M. Kleinschmidt, *WIREs Comput. Mol. Sci.* **2018**, *9*, 1.
- [30] N. Dupuy, M. Casula, *J. Chem. Phys.* **2018**, *148*, 134112.
- [31] a) F. Neese, *J. Phys. Chem. of Solids* **2004**, *65*, 781; b) F. Neese, *Coord. Chem. Rev.* **2009**, *253*, 526.
- [32] D. Fazzi, E. V. Canesi, F. Negri, C. Bertarelli, C. Castiglioni, *Chem. Phys. Chem.* **2010**, *11*, 3685.
- [33] S. Canola, J. Casado, F. Negri, *Phys. Chem. Chem. Phys.* **2018**, *20*, 24227.
- [34] a) M. Casula, C. Attaccalite, S. Sorella, *J. Chem. Phys.* **2004**, *121*, 7110; b) K. Nakano, C. Attaccalite, M. Barborini, L. Capriotti, M. Casula, E. Coccia, M. Dagrada, C. Genovese, Y. Luo, G. Mazzola, A. Zen, S. Sorella, *J. Chem. Phys.* **2020**, *152*, 204121.
- [35] F. Plasser, H. Pašalić, M. H. Gerzabek, F. Libisch, R. Reiter, J. Burgdörfer, T. Müller, R. Shepard, H. Lischka, *Angew. Chem. Int. Ed.* **2013**, *52*, 2581.
- [36] S. Grimme, A. Hansen, *Angew. Chem. Int. Ed.* **2015**, *54*, 12308.
- [37] C. A. Bauer, A. Hansen, S. Grimme, *Chem. Eur. J.* **2017**, *23*, 6150.
- [38] S. Canola, Y. Dai, F. Negri, *Computation* **2019**, *7*, 68.
- [39] a) I. H. Nayyar, E. R. Batista, S. Tretiak, A. Saxena, D. L. Smith, R. L. Martin, *J. Chem. Theo. Comput.* **2013**, *9*, 1144; b) M. Anderson, C. Ramanan, C. Fontanesi, A. Frick, S. Surana, D. Cheyns, M. Furno, T. Keller, S. Allard, U. Scherf, D. Beljonne, G. D'Avino, E. von Hauff, E. Da Como, *Phys. Rev. Mater.* **2017**, *1*, 055604; c) D. Fazzi, M. Caironi, C. Castiglioni, *J. Am. Chem. Soc.* **2011**, *133*, 19056.
- [40] N. A. Deskins, M. Dupuis, *Phys. Rev. B* **2007**, *75*, 195212.
- [41] A. L. Briseno, S. C. B. Mannsfeld, P. J. Shamberger, F. S. Ohuchi, Z. Bao, S. A. Jenekhe, Y. Xia, *Chem. Mat.* **2008**, *20*, 4712.
- [42] a) W. J. Kendrick, M. Jirásek, M. D. Peeks, G. M. Greetham, I. V. Sazanovich, P. M. Donaldson, M. Towrie, A. W. Parker, H. L. Anderson, *Chem. Sci.* **2020**, *11*, 2112; b) S. Kahmann, D. Fazzi, G. J. Matt, W. Thiel, M. A. Loi, C. J. Brabec, *J. Phys. Chem. Lett.* **2016**, *7*, 4438.

TOC

Multiple redox states are responsible for different conductive regimes that **BBL** features upon doping. Polarons are investigated *via* quantum-chemical modelling, revealing the multireference character of their wavefunctions. High conductive regimes are assigned to electron polaron and redox species carrying 0.75 electron per repeat unit. Insulating states refer to bipolaron (0.5eru) and species with 1eru.

Daniele Fazzi^{*1}, Fabrizia Negri²

Addressing the elusive polaronic nature of multiple redox states in a π -conjugated ladder-type polymer.



Supporting Information

Addressing the elusive polaronic nature of multiple redox states in a π -conjugated ladder-type polymer.

*Daniele Fazzi,^{*1} Fabrizia Negri²*

COMPUTATIONAL DETAILS

All calculations were performed via an oligomer approach. Oligomers from length $n = 1$ to 8 were considered. Each structure was optimized by using the hybrid range-separated-corrected DFT functional, namely ω B97X-D combined with double-zeta (and in some cases triple-zeta) split valence polarized Pope's basis set 6-31G* (6-311G*). The choice of ω B97X-D was due to its well-known superior performance in describing charged and excited states in conjugated polymers.¹⁻³ The effects of considering either B3LYP or a double hybrid DFT functional (e.g., B2PLYP), as well as an augmented basis set (e.g., 6-311+G*), were tested previously.⁴ Results did not show improvements with respect to ω B97X-D/6-31G* approach, and similar conclusion regarding the DFT instability in describing charged states can be drawn.

The electronic states investigated here were the neutral ground ($q = 0e$), the single negatively/positively charged states ($q = \pm 1e$), and the double negatively/positively charged ($q = \pm 2e$) states. Such states are referred to as polaron and bipolaron. A polaron shows a doublet state spin multiplicity (D), while a bipolaron can be either a singlet (S) or a triplet (T) state. Polarons were initially described using the UDFT approach, whereas for bipolarons the singlet was described using the RDFT and triplet the UDFT approaches. For each case, a wavefunction stability check was run using the BS-UDFT scheme. The BS scheme can be computed directly in Gaussian16 code by running a single-point calculations combining the

keywords `guess=mix` and `stable=opt`. In ORCA code, a similar approach is introduced by using the following keywords for the `%scf` block (example below):

```
%scf
guess hcore
HFTyp UHF
STABPerform true
STABRestartUHFifUnstable true
STABNRroots 3
STABMaxDim 3
STABMaxIter 500
end
```

If an instability in the wavefunction was found, both the electronic and nuclear structures were re-optimized following the BS-UDFT potential energy surface (namely, by restarting the calculation with the BS wavefunction obtained in the previous step (`guess=read` in Gaussian or `MORRead` keyword in ORCA)). All calculations were performed with the program package Gaussian16 B.01⁵ and ORCA v4.2.0.

Extra (multiple) charged states were investigated, namely $q = 3e^-$ and $q = 4e^-$. Such states are characterized by different state multiplicities, namely quartet (Q) and doublet (D) for $q = 3e^-$, and quintet (Qui), triplet (T) and singlet (S) for $q = 4e^-$. For each state, broken-symmetry stability check for the DFT wavefunction was performed.

In general, we considered (for each oligomer length) a variety of multiple charged states, encompassing polaron, bipolaron or extra charges up to one charge per repeat unit (depending on the oligomer length).

Specifically, we considered the following charged cases:

- BBL1: $q = 0, \pm 1, \pm 2$
- BBL2: $q = 0, \pm 1, \pm 2$
- BBL3: $q = 0, \pm 1, \pm 2, -3$
- BBL4: $q = 0, \pm 1, \pm 2, -3, -4$
- BBL5: $q = 0, \pm 1, \pm 2, -3, -4, -5$

- BBL6-8: $q=0, \pm 1, \pm 2$

Focus of the computational investigation was the modelling of hole/electron polaron (± 1), bipolaron (± 2) for all BBL oligomers, and multiple charged (i.e., negative) states for some of them, specifically for BBL4 considered to be the reference model system (as discussed in the main text) for the interpretation of the experimental spectro-electrochemical data.

FOD and CASSCF/NEVPT2 calculations (with def2-TZVP basis set) were performed by using ORCA v 4.2.0.

1. U. Salzner and A. Aydin, *J. Chem. Theory Comput.*, **2011**, 7, 2568–2583.
2. R. Baer, E. Livshits and U. Salzner, *Annu. Rev. Phys. Chem.*, **2010**, 61, 85–109.
3. U. Salzner, *Wiley Interdiscip. Rev.: Comput. Mol. Sci.*, **2014**, 4, 601–622.
4. D. Fazzi, et al., *J. Mater. Chem. C*, **2019**, 7, 12876–12885.
5. M. J. Frisch, G. W. Trucks, H. B. Schlegel, G. E. Scuseria, M. A. Robb, J. R. Cheeseman, G. Scalmani, V. Barone, G. A. Petersson, H. Nakatsuji, X. Li, M. Caricato, A. V. Marenich, J. Bloino, B. G. Janesko, R. Gomperts, B. Mennucci, H. P. Hratchian, J. V. Ortiz, A. F. Izmaylov, J. L. Sonnenberg, D. Williams-Young, F. Ding, F. Lipparini, F. Egidi, J. Goings, B. Peng, A. Petrone, T. Henderson, D. Ranasinghe, V. G. Zakrzewski, J. Gao, N. Rega, G. Zheng, W. Liang, M. Hada, M. Ehara, K. Toyota, R. Fukuda, J. Hasegawa, M. Ishida, T. Nakajima, Y. Honda, O. Kitao, H. Nakai, T. Vreven, K. Throssell, J. A. Montgomery, Jr., J. E. Peralta, F. Ogliaro, M. J. Bearpark, J. J. Heyd, E. N. Brothers, K. N. Kudin, V. N. Staroverov, T. A. Keith, R. Kobayashi, J. Normand, K. Raghavachari, A. P. Rendell, J. C. Burant, S. S. Iyengar, J. Tomasi, M. Cossi, J. M. Millam, M. Klene, C. Adamo, R. Cammi, J. W. Ochterski, R. L. Martin, K. Morokuma, O. Farkas, J. B. Foresman and D. J. Fox, Gaussian 16, Revision B.01, Gaussian, Inc., Wallingford CT, 2016.

Molecular Orbital (MO) analysis for BBL1-4.

In **Figure S1** are reported the MO energies for BBL1-4, together with the computed HOMO/HOMO-1 and LUMO/LUMO+1 gaps (in eV, see inset) and the FOD number (N_{FOD}). Calculations refer to ω B96X-D/6-31G* data.

FOD calculations were performed by using the standard (as implemented in ORCA) TPSS functional, or ω B96X-D with def2-SVP and/or def2-TZVP, both leading to similar results.

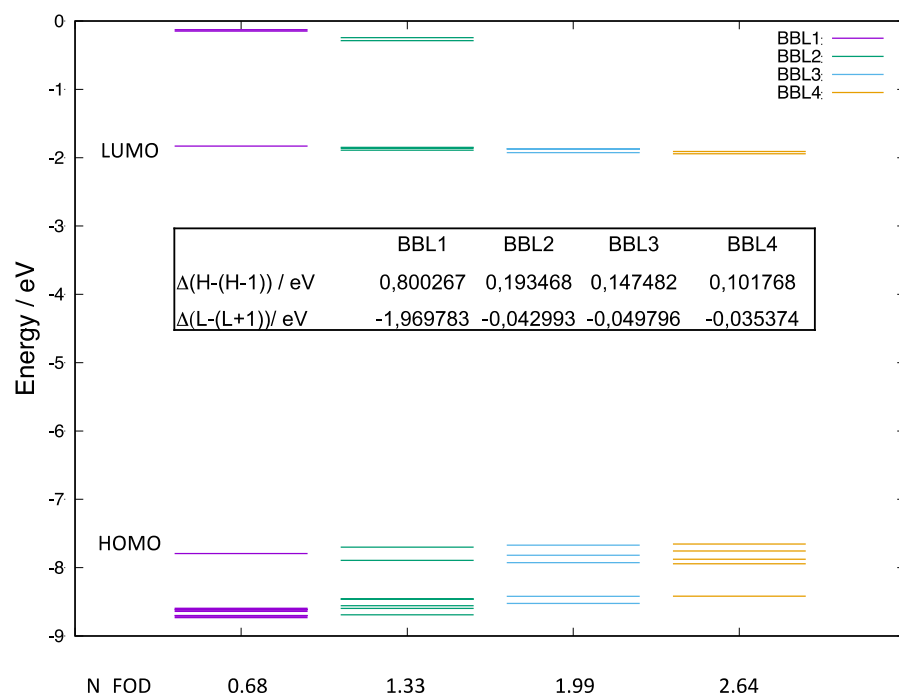


Figure S1

In **Figure S2** are reported the MOs (ω B96X-D/6-31G*) for BBL4 *cis* neutral.

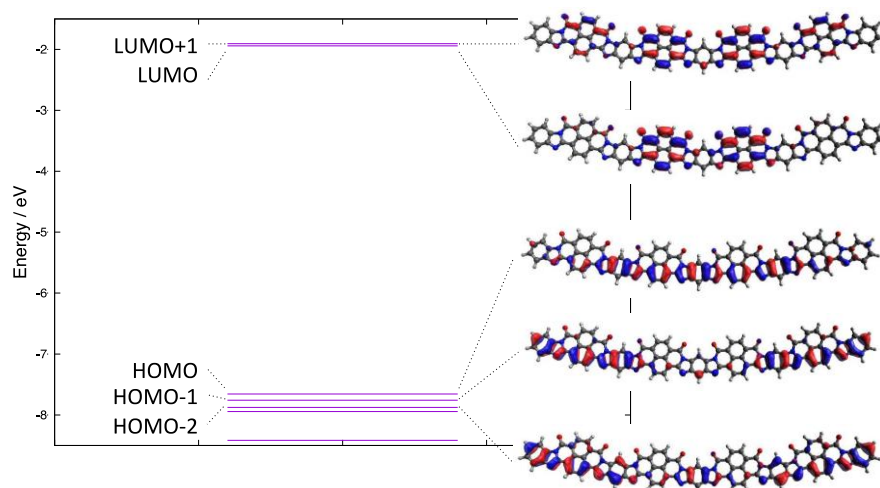


Figure S2

List of frontier MOs and respective fractional occupation number for BBL4 *cis* neutral species,
as computed in the FOD analysis.

NO	OCC	
...		
340	1.9864	
341	1.9853	
342	1.9848	
343	1.9846	
344	1.9842	
345	1.9838	
346	1.9835	
347	1.9833	
348	1.9832	
349	1.9830	
350	1.9826	
351	1.9637	
352	1.9611	
353	1.9555	
354	1.9492	
355	1.9357	
356	1.9279	
357	1.8510	
358	1.8386	
359	1.8035	
360	1.7611	# HOMO
361	0.3312	# LUMO
362	0.3128	
363	0.2939	
364	0.2840	
365	0.0249	
366	0.0182	
367	0.0112	
368	0.0065	
369	0.0062	
370	0.0054	
371	0.0041	
372	0.0038	
373	0.0033	
374	0.0033	
375	0.0033	
376	0.0033	
377	0.0020	
...		

DETAILS OF THE CASSCF/NEVPT2 CALCULATIONS PERFORMED ON BBL1

BBL1 shows stable DFT solutions for the neutral, singly charged $P_{\pm}(D)$ and electron doubly charged $B-(S)$ states, however a DFT instability was found for the hole bipolaron $B+(S)$ state, leading to a BS-UDFT ground state ([Figure 1](#) main text). Accordingly, the FOD analysis highlights a weak MR character for the neutral (N , $N_{FOD} < 0.7$) and electron charged ($P-$ and $B-$, $N_{FOD} < 0.8$) species ([Table 1](#) main text), while higher MR characters are predicted for the positive charged states, both polaron ($P+$, $N_{FOD} > 1.5$) and, especially, bipolaron ($B+$, $N_{FOD} > 2.0$).

We performed CASSCF/NEVPT2 calculations (see Supporting Information) for both electron and hole bipolarons ($B-(S)$ and $B+(S)$) to clearly address the presence (or not) of MR characters, therefore to correlate such aspects with the appearance (or not) of BS-UDFT solutions. CASSCF wavefunction for BBL1 $B+(S)$ undoubtedly indicate a strong contribution of doubly excited determinants (i.e., $H,H \rightarrow L,L$ - with H the highest occupied molecular orbital and L lowest one) in the description of the ground state ($\sim 40\%$), highlighting its pronounced MR character. For such state a low energy BS-UDFT solution was indeed found ([Figure 1](#) main text). On the contrary, the CASSCF wavefunction for the electron bipolaron $B-(S)$ revealed only negligible contributions ($< 9\%$) of doubly excited configurations to the ground state. The latter was found stable at the DFT level, without reporting any BS-UDFT solution ([Figure 1](#) main text).

***trans*, BIPOLARON ($q = \pm 2e$).**

Hole bipolaron ($q=+2e$) species

CASSCF/NEVPT2 with def2-TZVP basis set on top of DFT BS geometry.

CAS space: (10,12) - 10 electrons in 12 orbitals.

Ground state wavefunction composition highlighting the HOMO/LUMO orbitals and the doubly excited determinant.

```
ROOT 0:
0.46762: 222220000000
0.37514: 222202000000
0.01928: 212221000000
0.00892: 222112000000
0.00875: 212211100000
0.00670: 112220100100
0.00592: 221120011000
0.00586: 221211001000
0.00580: 222111010000
0.00473: 221102011000
0.00439: 112202100100
0.00415: 022220000200
0.00412: 202220200000
0.00332: 022202000200
0.00257: 202202200000
```

Electron bipolaron ($q=-2e$) species

CASSCF/NEVPT2 with def2-TZVP basis set on top of DFT geometry.

CAS space: (8,9)

Ground state wavefunction composition highlighting the HOMO/LUMO orbitals and the doubly excited determinant.

```
ROOT 0:
0.95322: 222200000
0.01376: 222020000
0.00719: 212111000
0.00447: 221110100
0.00366: 222002000
```


IR SPECTROSCOPIC ASSIGNMENTS

Experimental FT-IR data are taken from T. Yohannes et al., *J. Phys. Chem. B* **2000**, 104, 9430-9437.

Computed frequencies (scaled values are reported, scale factor 0.93, level of theory ω B97X-D/6-31G*) refer to BBL4 *cis*.

Neutral species

v expt. cm ⁻¹	v theo. cm ⁻¹	Assignment
1703	1711-1705 (six active IR normal modes)	CO asymmetric stretching
1500	1543	CC str. + CN str.
1370	1388	CH rocking
1320	1321	quinoidal mode on benzimidazole + CN str.
1237	1275	quinoidal mode on benzimidazole + CN str.
1171	1171	CH rocking

Charged species Species A, $q = 1e^-$ (0.25e_{ru})

Computed values refer to the BS-UDFT geometry (polaron P-, D-BS state).

v expt. cm ⁻¹	v theo. cm ⁻¹	Assignment
1649	1640	CO asymmetric stretching localized on one benzophenanthroline unit (polaron localisation)
1522	1503	quinoidal mode on benzophenanthroline + CN str.
1255	1273	CH rocking + CN str.
1150	1170	quinoidal mode on benzimidazole + CN str.

Charged species

Species B, $q = 2e^-$ (0.50e_{ru})

Computed values refer to the BS-UDFT geometry (bipolaron B⁻, S-BS state).

ν expt. cm ⁻¹	ν theo. cm ⁻¹	Assignment
1614	1635	CO asymmetric stretching localized on two units (bipolaron localisation)
not reported	1501	quinoidal mode on benzophenanthroline + CN str.
1278	1272	quinoidal mode on benzimidazole + CN str.
1219	1241	
1099	1169	CH rocking + CN str.
1028		<i>spurious bands associated to a protonated species (see manuscript)</i>

Charged species

Species C, $q = 3e^-$ (0.75 e^-)

Computed values refer to the BS-UDFT geometry (Quartet, Q-BS state).

ν expt. cm^{-1}	ν theo. cm^{-1}	Assignment
not reported	1627	CO asymmetric stretching localized on one unit
1509	1500	quinoidal mode on benzophenanthroline + CN str.
1369	1360	CH rocking on benzimidazole + CN str. + quinoidal mode on benzophenanthroline
1070	1169	CH rocking on benzophenanthroline

Charged species

Species D, $q = 4e^-$ (1eru)

Computed values refer to the UDFT geometry (Quintet, Qui).

v expt. cm ⁻¹	v theo. cm ⁻¹	Assignment
1593	1620	CO asymmetric stretching localized on two units
not reported	1469	quinoidal mode on benzophenanthroline + CN str.
1363	1359	CH rocking on benzimidazole + CN str.
not reported	1170	CH rocking on benzophenanthroline

COMPUTED IR SPECTRA FOR EACH STATE SPIN MULTIPLICITIES

Computed IR spectra (ω belonging to the same charged state but differing for their spin multiplicity. Differences are almost imperceptible and IR spectra basically overlap.

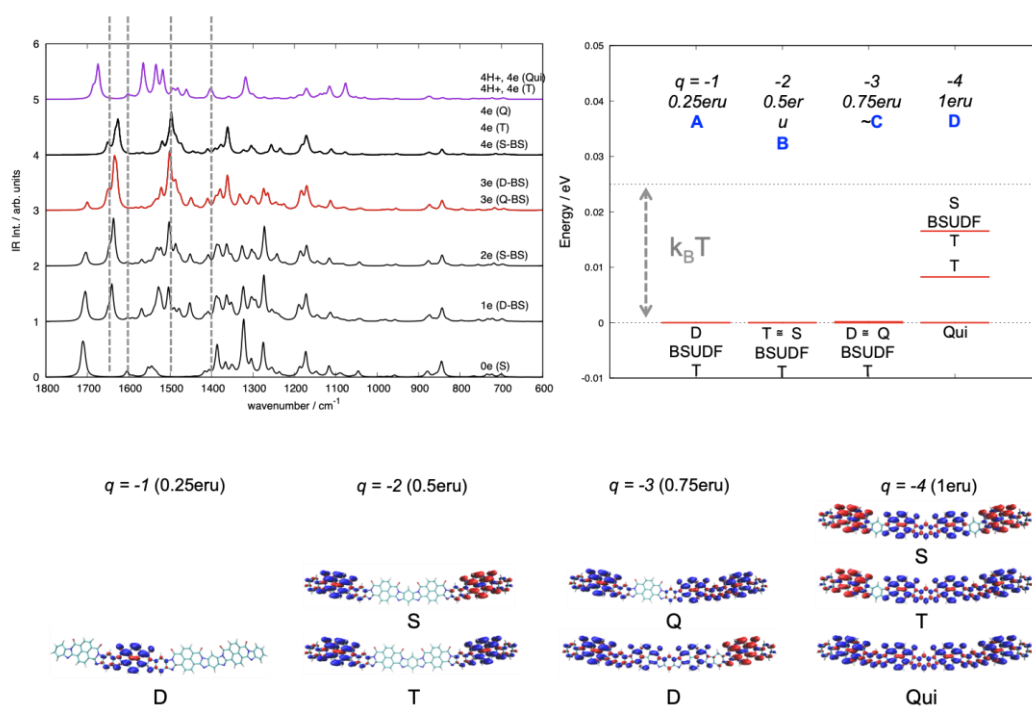


Figure S3

COMPARISON BETWEEN COMPUTED EXCITED STATES FOR *cis* AND *trans* CONFORMER (case of BBL4).

Here below are reported the computed (TDDFT, ω B97X-D/6-31G*) excitation energies for each species of BBL4, *cis* and *trans* conformers (most stable state is shown). BS indicates the use of a BS wavefunction on top of a BS optimized geometries.

BBL4 *cis*, P- (D) – TD-BS-UDFT

Excited State	1	1.1476 eV	1080.34 nm	f= 0.0055	<S**2>=0.850
Excited State	2	1.2288 eV	1008.97 nm	f= 0.0074	<S**2>=0.855
Excited State	3	1.2994 eV	954.20 nm	f= 0.0001	<S**2>=0.787
Excited State	4	1.5893 eV	780.13 nm	f= 0.0001	<S**2>=2.766
Excited State	5	1.5988 eV	775.50 nm	f= 0.0001	<S**2>=2.765
Excited State	6	1.6874 eV	734.77 nm	f= 0.0000	<S**2>=2.776
Excited State	7	1.9242 eV	644.35 nm	f= 0.0288	<S**2>=0.818
Excited State	8	2.1633 eV	573.13 nm	f= 0.4991	<S**2>=1.062
Excited State	9	2.4098 eV	514.50 nm	f= 0.1844	<S**2>=1.996
Excited State	10	2.4643 eV	503.12 nm	f= 0.1822	<S**2>=2.045
Excited State	11	2.5176 eV	492.47 nm	f= 2.3441	<S**2>=1.363
Excited State	12	2.6086 eV	475.29 nm	f= 0.1113	<S**2>=1.277
Excited State	13	2.6391 eV	469.80 nm	f= 0.0018	<S**2>=2.376
Excited State	14	2.6619 eV	465.77 nm	f= 0.0088	<S**2>=2.365
Excited State	15	2.7034 eV	458.63 nm	f= 0.2845	<S**2>=1.087
Excited State	16	2.7099 eV	457.52 nm	f= 0.2046	<S**2>=1.611
Excited State	17	2.8442 eV	435.92 nm	f= 0.0050	<S**2>=2.732
Excited State	18	2.8529 eV	434.59 nm	f= 0.4027	<S**2>=0.916
Excited State	19	2.8924 eV	428.65 nm	f= 0.1354	<S**2>=0.920
Excited State	20	2.9215 eV	424.38 nm	f= 0.1566	<S**2>=0.994
Excited State	21	2.9422 eV	421.40 nm	f= 0.0915	<S**2>=2.290
Excited State	22	2.9668 eV	417.90 nm	f= 0.0911	<S**2>=1.490
Excited State	23	2.9802 eV	416.03 nm	f= 0.0044	<S**2>=1.792
Excited State	24	3.0491 eV	406.63 nm	f= 0.0000	<S**2>=2.721
Excited State	25	3.0576 eV	405.50 nm	f= 0.0048	<S**2>=2.598

BBL4 *cis*, B- (S) – TD-BS-UDFT

Excited State	1	1.2779 eV	970.20 nm	f= 0.0091	<S**2>=1.134
Excited State	2	1.2781 eV	970.06 nm	f= 0.0033	<S**2>=1.133
Excited State	3	1.5925 eV	778.56 nm	f= 0.0001	<S**2>=3.043
Excited State	4	1.6210 eV	764.86 nm	f= 0.0001	<S**2>=3.042
Excited State	5	1.9724 eV	628.58 nm	f= 0.0130	<S**2>=1.091
Excited State	6	1.9731 eV	628.36 nm	f= 0.0773	<S**2>=1.091
Excited State	7	2.0845 eV	594.79 nm	f= 0.0002	<S**2>=1.063
Excited State	8	2.0846 eV	594.77 nm	f= 0.0018	<S**2>=1.063
Excited State	9	2.1717 eV	570.92 nm	f= 0.5858	<S**2>=1.276
Excited State	10	2.1770 eV	569.52 nm	f= 0.0120	<S**2>=1.276
Excited State	11	2.4866 eV	498.60 nm	f= 0.8740	<S**2>=1.961
Excited State	12	2.5034 eV	495.26 nm	f= 0.0071	<S**2>=2.383
Excited State	13	2.5827 eV	480.06 nm	f= 2.2723	<S**2>=1.885
Excited State	14	2.6489 eV	468.05 nm	f= 0.0209	<S**2>=1.521
Excited State	15	2.6655 eV	465.14 nm	f= 0.0005	<S**2>=2.820
Excited State	16	2.6933 eV	460.35 nm	f= 0.0006	<S**2>=2.481

Excited State	17	2.7032 eV	458.66 nm	f= 0.0927	<S**2>=1.367
Excited State	18	2.7067 eV	458.07 nm	f= 0.0029	<S**2>=1.485
Excited State	19	2.7367 eV	453.04 nm	f= 0.6569	<S**2>=1.354
Excited State	20	2.7417 eV	452.22 nm	f= 0.0136	<S**2>=1.554

BBL4 cis, q=3e- (D) – TD-BS-UDFT

Excited State	1	1.1842 eV	1046.95 nm	f= 0.0086	<S**2>=1.919
Excited State	2	1.5807 eV	784.38 nm	f= 0.0001	<S**2>=3.822
Excited State	3	1.8712 eV	662.59 nm	f= 0.0224	<S**2>=1.915
Excited State	4	1.9328 eV	641.47 nm	f= 0.0546	<S**2>=1.882
Excited State	5	1.9984 eV	620.43 nm	f= 0.0343	<S**2>=1.875
Excited State	6	2.0760 eV	597.22 nm	f= 0.0023	<S**2>=1.849
Excited State	7	2.0810 eV	595.79 nm	f= 0.0192	<S**2>=1.906
Excited State	8	2.1351 eV	580.70 nm	f= 0.9879	<S**2>=2.057
Excited State	9	2.1587 eV	574.34 nm	f= 0.0213	<S**2>=2.060
Excited State	10	2.1767 eV	569.59 nm	f= 0.1321	<S**2>=2.048
Excited State	11	2.4421 eV	507.70 nm	f= 0.3599	<S**2>=2.895
Excited State	12	2.5707 eV	482.30 nm	f= 2.2852	<S**2>=2.472
Excited State	13	2.6622 eV	465.71 nm	f= 0.1269	<S**2>=2.853
Excited State	14	2.6713 eV	464.13 nm	f= 0.1080	<S**2>=2.167
Excited State	15	2.6750 eV	463.48 nm	f= 0.0793	<S**2>=2.033
Excited State	16	2.6866 eV	461.50 nm	f= 0.0288	<S**2>=2.065
Excited State	17	2.6950 eV	460.06 nm	f= 0.2610	<S**2>=2.725
Excited State	18	2.7469 eV	451.36 nm	f= 0.3780	<S**2>=2.156
Excited State	19	2.7858 eV	445.06 nm	f= 0.0132	<S**2>=2.049
Excited State	20	2.8100 eV	441.22 nm	f= 0.0004	<S**2>=1.078
Excited State	21	2.8829 eV	430.06 nm	f= 0.0165	<S**2>=3.713
Excited State	22	2.9353 eV	422.39 nm	f= 0.0415	<S**2>=1.931
Excited State	23	2.9749 eV	416.77 nm	f= 0.0717	<S**2>=3.395
Excited State	24	2.9938 eV	414.14 nm	f= 0.0245	<S**2>=2.641
Excited State	25	3.0727 eV	403.50 nm	f= 0.1824	<S**2>=2.677
Excited State	26	3.1228 eV	397.03 nm	f= 0.0003	<S**2>=0.894
Excited State	27	3.1727 eV	390.78 nm	f= 0.0253	<S**2>=2.784
Excited State	28	3.2007 eV	387.37 nm	f= 0.1060	<S**2>=2.558
Excited State	29	3.2900 eV	376.85 nm	f= 0.0096	<S**2>=2.309
Excited State	30	3.3172 eV	373.77 nm	f= 0.0375	<S**2>=2.678

BBL4 cis, q=4e- (Qui) – TD-BS-UDFT

Excited State	1	1.9728 eV	628.48 nm	f= 0.0795	<S**2>=6.171
Excited State	2	1.9761 eV	627.43 nm	f= 0.0244	<S**2>=6.165
Excited State	3	1.9910 eV	622.71 nm	f= 0.0360	<S**2>=6.165
Excited State	4	1.9922 eV	622.34 nm	f= 0.0171	<S**2>=6.160
Excited State	5	2.1023 eV	589.75 nm	f= 1.6080	<S**2>=6.328
Excited State	6	2.1384 eV	579.79 nm	f= 0.0394	<S**2>=6.332
Excited State	7	2.1441 eV	578.27 nm	f= 0.0010	<S**2>=6.349
Excited State	8	2.1475 eV	577.33 nm	f= 0.0000	<S**2>=6.336
Excited State	9	2.6240 eV	472.50 nm	f= 2.3877	<S**2>=6.232
Excited State	10	2.6325 eV	470.98 nm	f= 0.5982	<S**2>=6.349
Excited State	11	2.6334 eV	470.81 nm	f= 0.0004	<S**2>=6.299
Excited State	12	2.6697 eV	464.42 nm	f= 0.0000	<S**2>=6.329
Excited State	13	2.6706 eV	464.26 nm	f= 0.0441	<S**2>=6.303
Excited State	14	2.7037 eV	458.57 nm	f= 0.0469	<S**2>=6.311
Excited State	15	2.7753 eV	446.73 nm	f= 0.0352	<S**2>=6.357
Excited State	16	2.8258 eV	438.76 nm	f= 0.0006	<S**2>=6.354
Excited State	17	2.9739 eV	416.90 nm	f= 0.0124	<S**2>=6.876
Excited State	18	2.9740 eV	416.89 nm	f= 0.0487	<S**2>=6.888
Excited State	19	3.0314 eV	409.00 nm	f= 0.0023	<S**2>=7.261
Excited State	20	3.0565 eV	405.65 nm	f= 0.2085	<S**2>=6.674
Excited State	21	3.0639 eV	404.66 nm	f= 0.0098	<S**2>=6.584

Excited State	22	3.1414 eV	394.68 nm	f= 0.6020	<S**2>=6.730
Excited State	23	3.2228 eV	384.71 nm	f= 0.0123	<S**2>=6.949
Excited State	24	3.2765 eV	378.41 nm	f= 0.0428	<S**2>=7.061
Excited State	25	3.3293 eV	372.41 nm	f= 0.0025	<S**2>=7.161
Excited State	26	3.3299 eV	372.34 nm	f= 0.0130	<S**2>=6.785
Excited State	27	3.3854 eV	366.23 nm	f= 0.0002	<S**2>=6.433
Excited State	28	3.4258 eV	361.91 nm	f= 0.0449	<S**2>=6.812
Excited State	29	3.5210 eV	352.13 nm	f= 0.0010	<S**2>=6.495
Excited State	30	3.5556 eV	348.71 nm	f= 0.0046	<S**2>=6.400

BBL4 trans, P- (D) – TD-BS-UDFT

Excited State	1	0.9720 eV	1275.60 nm	f= 0.5538	<S**2>=1.073
Excited State	2	1.1415 eV	1086.16 nm	f= 0.1101	<S**2>=1.208
Excited State	3	1.3918 eV	890.82 nm	f= 0.0022	<S**2>=0.946
Excited State	4	1.6345 eV	758.53 nm	f= 0.2407	<S**2>=2.423
Excited State	5	1.6903 eV	733.50 nm	f= 0.1389	<S**2>=2.353
Excited State	6	1.7339 eV	715.06 nm	f= 0.0289	<S**2>=2.612
Excited State	7	1.9736 eV	628.23 nm	f= 0.0261	<S**2>=0.842
Excited State	8	2.0999 eV	590.43 nm	f= 0.9297	<S**2>=1.120
Excited State	9	2.3182 eV	534.83 nm	f= 0.0031	<S**2>=2.555
Excited State	10	2.4074 eV	515.02 nm	f= 0.0238	<S**2>=2.499
Excited State	11	2.5254 eV	490.95 nm	f= 1.0964	<S**2>=0.969
Excited State	12	2.5776 eV	481.01 nm	f= 0.3449	<S**2>=2.309
Excited State	13	2.6102 eV	475.01 nm	f= 0.3450	<S**2>=1.213
Excited State	14	2.7157 eV	456.54 nm	f= 0.0043	<S**2>=1.368
Excited State	15	2.7803 eV	445.94 nm	f= 0.0012	<S**2>=2.117
Excited State	16	2.8088 eV	441.41 nm	f= 0.0008	<S**2>=1.670
Excited State	17	2.8492 eV	435.15 nm	f= 0.0025	<S**2>=2.281
Excited State	18	2.9079 eV	426.37 nm	f= 0.0458	<S**2>=1.230
Excited State	19	2.9542 eV	419.69 nm	f= 0.9844	<S**2>=0.824
Excited State	20	3.0308 eV	409.08 nm	f= 0.0001	<S**2>=2.553

BBL4 trans, B- (D) – TD-BS-UDFT

Excited State	1	1.0841 eV	1143.61 nm	f= 0.6503	<S**2>=1.441
Excited State	2	1.1021 eV	1124.97 nm	f= 0.0000	<S**2>=1.503
Excited State	3	1.6625 eV	745.79 nm	f= 0.0000	<S**2>=2.622
Excited State	4	1.7015 eV	728.67 nm	f= 0.4193	<S**2>=2.614
Excited State	5	1.9622 eV	631.88 nm	f= 0.0890	<S**2>=1.095
Excited State	6	1.9625 eV	631.77 nm	f= 0.0000	<S**2>=1.098
Excited State	7	2.1123 eV	586.97 nm	f= 0.0000	<S**2>=1.413
Excited State	8	2.1432 eV	578.49 nm	f= 0.0047	<S**2>=1.089
Excited State	9	2.1508 eV	576.44 nm	f= 1.0746	<S**2>=1.266
Excited State	10	2.1596 eV	574.10 nm	f= 0.0000	<S**2>=1.226
Excited State	11	2.3033 eV	538.30 nm	f= 0.0000	<S**2>=2.488
Excited State	12	2.4518 eV	505.68 nm	f= 0.1233	<S**2>=2.594
Excited State	13	2.5618 eV	483.98 nm	f= 2.2617	<S**2>=1.298
Excited State	14	2.6228 eV	472.72 nm	f= 0.0000	<S**2>=1.184
Excited State	15	2.6834 eV	462.04 nm	f= 0.0000	<S**2>=1.433
Excited State	16	2.6928 eV	460.43 nm	f= 0.0402	<S**2>=1.454
Excited State	17	2.7894 eV	444.48 nm	f= 0.2113	<S**2>=1.275
Excited State	18	2.7953 eV	443.54 nm	f= 0.0000	<S**2>=1.388
Excited State	19	2.8585 eV	433.73 nm	f= 0.0000	<S**2>=2.755
Excited State	20	2.8655 eV	432.68 nm	f= 0.0088	<S**2>=2.817
Excited State	21	2.9529 eV	419.88 nm	f= 0.0000	<S**2>=2.245
Excited State	22	3.0105 eV	411.84 nm	f= 0.0449	<S**2>=1.778
Excited State	23	3.0500 eV	406.50 nm	f= 0.0000	<S**2>=2.303
Excited State	24	3.0899 eV	401.26 nm	f= 0.2667	<S**2>=1.224
Excited State	25	3.1394 eV	394.93 nm	f= 0.0000	<S**2>=1.405
Excited State	26	3.1774 eV	390.20 nm	f= 0.1572	<S**2>=1.364

Excited State	27	3.2263 eV	384.29 nm	f= 0.0000	<S**2>=1.292
Excited State	28	3.2793 eV	378.08 nm	f= 0.3047	<S**2>=1.704
Excited State	29	3.3369 eV	371.55 nm	f= 0.0000	<S**2>=2.878
Excited State	30	3.3449 eV	370.66 nm	f= 0.0735	<S**2>=2.412

BBL4 trans, 3e- (D) – TD-BS-UDFT

Excited State	1	0.9938 eV	1247.56 nm	f= 0.4514	<S**2>=4.187
Excited State	2	1.5820 eV	783.70 nm	f= 0.0320	<S**2>=5.136
Excited State	3	1.8226 eV	680.26 nm	f= 0.8475	<S**2>=4.272
Excited State	4	1.8988 eV	652.95 nm	f= 0.0603	<S**2>=3.904
Excited State	5	1.9525 eV	634.99 nm	f= 0.0013	<S**2>=3.870
Excited State	6	2.0173 eV	614.60 nm	f= 0.5856	<S**2>=4.040
Excited State	7	2.0463 eV	605.88 nm	f= 0.1894	<S**2>=4.101
Excited State	8	2.1112 eV	587.26 nm	f= 0.0174	<S**2>=3.947
Excited State	9	2.1767 eV	569.61 nm	f= 0.4225	<S**2>=4.017
Excited State	10	2.2236 eV	557.58 nm	f= 0.0010	<S**2>=3.992
Excited State	11	2.3529 eV	526.95 nm	f= 0.0208	<S**2>=5.050
Excited State	12	2.5565 eV	484.98 nm	f= 1.4410	<S**2>=4.128
Excited State	13	2.5904 eV	478.63 nm	f= 0.5607	<S**2>=4.163
Excited State	14	2.6460 eV	468.57 nm	f= 0.0309	<S**2>=4.095
Excited State	15	2.6686 eV	464.60 nm	f= 0.0135	<S**2>=4.149
Excited State	16	2.7046 eV	458.41 nm	f= 0.0666	<S**2>=3.967
Excited State	17	2.7738 eV	446.98 nm	f= 0.7374	<S**2>=4.015
Excited State	18	2.8032 eV	442.29 nm	f= 0.0034	<S**2>=4.179
Excited State	19	2.8571 eV	433.95 nm	f= 0.0185	<S**2>=4.508
Excited State	20	2.8972 eV	427.95 nm	f= 0.0026	<S**2>=5.031
Excited State	21	2.9343 eV	422.53 nm	f= 0.0029	<S**2>=4.914
Excited State	22	3.0178 eV	410.84 nm	f= 0.0154	<S**2>=4.527
Excited State	23	3.0733 eV	403.42 nm	f= 0.0401	<S**2>=4.277
Excited State	24	3.1178 eV	397.67 nm	f= 0.0667	<S**2>=4.108
Excited State	25	3.1298 eV	396.14 nm	f= 0.0032	<S**2>=5.039
Excited State	26	3.2002 eV	387.43 nm	f= 0.0045	<S**2>=4.728
Excited State	27	3.2110 eV	386.13 nm	f= 0.0186	<S**2>=4.973
Excited State	28	3.2929 eV	376.52 nm	f= 0.0296	<S**2>=4.490
Excited State	29	3.3617 eV	368.81 nm	f= 0.0059	<S**2>=4.675
Excited State	30	3.4124 eV	363.34 nm	f= 0.0196	<S**2>=4.316

BBL4 trans, 4e- (S) – TD-BS-UDFT

Excited State	1	1.7090 eV	725.49 nm	f= 1.5923	<S**2>=1.805
Excited State	2	1.7520 eV	707.69 nm	f= 0.0000	<S**2>=1.762
Excited State	3	1.9240 eV	644.40 nm	f= 0.3149	<S**2>=2.131
Excited State	4	1.9326 eV	641.53 nm	f= 0.0000	<S**2>=2.153
Excited State	5	1.9975 eV	620.70 nm	f= 0.0000	<S**2>=2.044
Excited State	6	2.0080 eV	617.45 nm	f= 0.0117	<S**2>=2.026
Excited State	7	2.0881 eV	593.76 nm	f= 0.0000	<S**2>=2.129
Excited State	8	2.0973 eV	591.17 nm	f= 1.1994	<S**2>=2.199
Excited State	9	2.3385 eV	530.18 nm	f= 0.0739	<S**2>=1.944
Excited State	10	2.3440 eV	528.94 nm	f= 0.0000	<S**2>=1.908
Excited State	11	2.4937 eV	497.19 nm	f= 0.0000	<S**2>=2.388
Excited State	12	2.5727 eV	481.93 nm	f= 0.6514	<S**2>=1.900
Excited State	13	2.6127 eV	474.55 nm	f= 0.3877	<S**2>=2.399
Excited State	14	2.6431 eV	469.08 nm	f= 0.0000	<S**2>=2.363
Excited State	15	2.6478 eV	468.25 nm	f= 0.0332	<S**2>=2.326
Excited State	16	2.6970 eV	459.72 nm	f= 0.0000	<S**2>=2.150
Excited State	17	2.7227 eV	455.37 nm	f= 1.3577	<S**2>=2.157
Excited State	18	2.7669 eV	448.09 nm	f= 0.0000	<S**2>=2.238
Excited State	19	2.8549 eV	434.28 nm	f= 0.0173	<S**2>=2.552

Excited State	20	2.8731 eV	431.53 nm	f= 0.0000	<S**2>=2.400
Excited State	21	2.9295 eV	423.23 nm	f= 0.0000	<S**2>=2.416
Excited State	22	2.9708 eV	417.34 nm	f= 0.0590	<S**2>=2.172
Excited State	23	3.0536 eV	406.03 nm	f= 0.0000	<S**2>=2.312
Excited State	24	3.1121 eV	398.39 nm	f= 0.0823	<S**2>=2.303
Excited State	25	3.2614 eV	380.15 nm	f= 0.0000	<S**2>=2.712
Excited State	26	3.3112 eV	374.44 nm	f= 0.0269	<S**2>=2.490
Excited State	27	3.3423 eV	370.95 nm	f= 0.0000	<S**2>=2.570
Excited State	28	3.3878 eV	365.97 nm	f= 0.0000	<S**2>=2.876
Excited State	29	3.3934 eV	365.37 nm	f= 0.0065	<S**2>=2.607
Excited State	30	3.4680 eV	357.51 nm	f= 0.0116	<S**2>=2.762

IR ASSIGNMENT FOR THE PROTONATED SPECIES

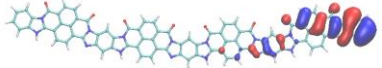
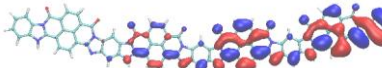
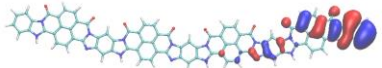
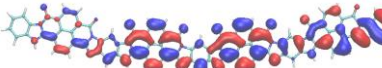
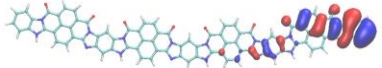
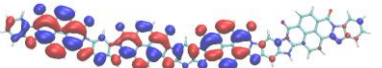
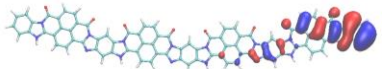
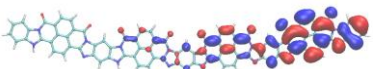
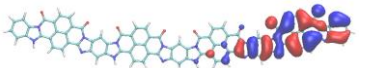
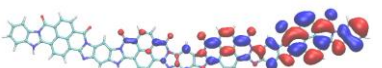
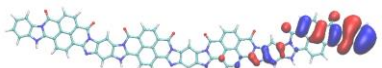
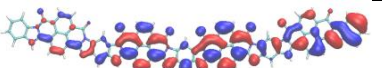
Most intense IR active band as computed (\square B97X-D/6-31G*) for BBL4 *cis* 4H⁺ (Quintet state).

ν theo. cm ⁻¹	Assignment
1692, 1698, 1700, 1704, 1729, 1729, 1747, 1752	8x CO str.
990	CH rocking coupled with NH rocking localised on one benzophenantroline

MOS FOR THE PROTONATED BBL4 4H⁺ SPECIES.

Molecular orbitals (beta) involved in the low-energy electronic transition (S1), as computed at the TD-DFT level (UωB97X-D/6-31G*, Quintet state) for BBL4 *cis* 4H⁺ (see Figure 6 of the manuscript).

S₁: E = 1.12 eV, f = 0.0517

Occ.	Virt.	Coeff.
 SOMO ₂ -2	 SUMO ₂ +1	0.67
 SOMO ₂ -2	 SUMO ₂ +2	-0.47
 SOMO ₂ -2	 SUMO ₂ +3	0.10
 SOMO ₂ -2	 SUMO ₂ +5	-0.28
 SOMO ₂	 SUMO ₂ +1	-0.35
 SOMO ₂ -2	 SUMO ₂ +2	0.23

- [1] a) J. Lee, A. J. Kalin, T. Yuan, M. Al-Hashimi, L. Fang, *Chem Sci* **2017**, 8, 2503; b) U. Scherf, *J. Mater. Chem.* **1999**, 9, 1853; c) R. S. Sprick, A. Thomas, U. Scherf, *Polymer Chemistry* **2010**, 1, 283; d) E. Khodabakhshi, C. Ramanan, J. J. Michels, S. Bonus, D. Hertel, K. Meerholz, M. Forster, U. Scherf, P. W. M. Blom, *Advanced Electronic Materials* **2020**, 6, 2000082; e) R. Lu, Y. Han, W. Zhang, X. Zhu, Z. Fei, T. Hodsdon, T. D. Anthopoulos, M. Heeney, *Journal of Materials Chemistry C* **2018**, 6, 2004; f) D. D. Igal Belaish, Henry Selig, Malcolm R. McLean, Larry Dalton, *Adv. Mater.* **1989**, 387; g) J. P. W. Graupner, J. Shinar, G. Leising, and U. Scherf, *Phys Rev Lett* **1996**, 77, 2033.
- [2] A.-D. Schlüter, *Advanced Materials* **1991**, 3, 282.
- [3] Y. Yin, S. Zhang, D. Chen, F. Guo, G. Yu, L. Zhao, Y. Zhang, *Polymer Chemistry* **2018**, 9, 2227.
- [4] R. L. V. Deusen, *Polymer Letters* **1966**, 4, 4.
- [5] M. C. Luping Yu, and Larry R. Dalton, *Chem. Mat.* **1990**, 2, 649.
- [6] a) A. Vogel, M. Forster, L. Wilbraham, C. L. Smith, A. J. Cowan, M. A. Zwijnenburg, R. S. Sprick, A. I. Cooper, *Faraday Discuss* **2019**, 215, 84; b) J. Lee, B. B. Rajeeva, T. Yuan, Z. H. Guo, Y. H. Lin, M. Al-Hashimi, Y. Zheng, L. Fang, *Chem Sci* **2016**, 7,

- 881; c) Y. Chen, H. Li, M. Tang, S. Zhuo, Y. Wu, E. Wang, S. Wang, C. Wang, W. Hu, *Journal of Materials Chemistry A* **2019**, 7, 20891.
- [7] E. J. L. Hidek Sibirakawa, Alan G. MacDiarmid, Chwan K. Chiang, and Alan J. Heeger, *J. C. S. Chem. Comm.* **1977**, 578.
- [8] O.-K. Kim, *Journal of Polymer Science: Polymer Letters Edition* **1982**, 20, 4.
- [9] O.-K. Kim, *Molecular Crystals and Liquid Crystals* **1984**, 105, 161.
- [10] K. W. a. R. W. Murray, *Macromolecules* **1988**, 21, 8.
- [11] F. B. T. Zheng, I.M. Brown, D.J. Leopold, T.C. Sandreczki, *Synthetic Metals* **1999**, 107, 7.
- [12] H. N. T. Yohannes, S. Luzzati, M. Catellani, S. Yi., S. A. Jenekhe, N. S. Sariciftci., *Synthetic Metals* **2001**, 119, 319.
- [13] K. W. a. R. W. Murray, *J. Phys. Chem.* **1988**, 92, 3642.
- [14] H. N. Teketel Yohannes, Silvia Luzzati, Marinella Catellani, Samson A. Jenekhe, and N. Serdar Sariciftci, *J. Phys. Chem. B* **2000**, 104, 8.
- [15] a) H. Antoniadis, M. A. Abkowitz, J. A. Osaheni, S. A. Jenekhe, M. Stolka, *Chem. Mat.* **1994**, 6, 63; b) S. A. J. Maksudul M. Alam, *J. Phys. Chem. B* **2002**, 106, 6.
- [16] a) A. B. a. S. A. Jenekhe, *J. Am. Chem. Soc.* **2003**, 125, 2; b) A. L. Briseno, F. S. Kim, A. Babel, Y. Xia, S. A. Jenekhe, *Journal of Materials Chemistry* **2011**, 21, 16461; c) H. Sun, J. Gerasimov, M. Berggren, S. Fabiano, *Journal of Materials Chemistry C* **2018**, 6, 11778.
- [17] S. A. Jenekhe, S. Yi, *Applied Physics Letters* **2000**, 77, 2635.
- [18] S. Wang, H. Sun, U. Ail, M. Vagin, P. O. Persson, J. W. Andreasen, W. Thiel, M. Berggren, X. Crispin, D. Fazzi, S. Fabiano, *Adv Mater* **2016**, 28, 10764.
- [19] a) J. Wu, X. Rui, C. Wang, W.-B. Pei, R. Lau, Q. Yan, Q. Zhang, *Advanced Energy Materials* **2015**, 5, 1402189; b) W. C. Jian Xie, Zilong Wang, Kenneth Choo Wei Jie, Ming Liu, and Qichun Zhang, *Chem. Asian J.* **2017**, 12, 9.
- [20] a) S. A. J. X. Linda Chen, *Macromolecules* **1997**, 30, 6; b) K. Xu, H. Sun, T.-P. Ruoko, G. Wang, R. Kroon, N. B. Kolhe, Y. Puttisong, X. Liu, D. Fazzi, K. Shibata, C.-Y. Yang, N. Sun, G. Persson, A. B. Yankovich, E. Olsson, H. Yoshida, W. M. Chen, M. Fahlman, M. Kemerink, S. A. Jenekhe, C. Müller, M. Berggren, S. Fabiano, *Nature materials* **2020**, 19, 738.
- [21] M. K. Sung Y. Hong, Yong S. Lee and Oh-Kil Kim, *Macromolecules* **1992**, 25, 6.
- [22] S. Ghosh, V. Gueskine, M. Berggren, I. V. Zozoulenko, *The Journal of Physical Chemistry C* **2019**, 123, 15467.
- [23] a) A. S. Igor Zozoulenko, Sandeep Kumar Singh, Viktor Gueskine, Xavier Crispin, Magnus Berggren, *ACS Appl. Polym. Mater.* **2019**, 1, 12; b) G. B. S. J. L. Brédas, *Accounts of chemical research* **1985**, 18, 7; c) J. Li, G. D'Avino, A. Pershin, D. Jacquemin, I. Duchemin, D. Beljonne, X. Blase, *Physical Review Materials* **2017**, 1.
- [24] D. Fazzi, S. Fabiano, T.-P. Ruoko, K. Meerholz, F. Negri, *Journal of Materials Chemistry C* **2019**, 7, 12876.
- [25] J. P. Perdew, A. Savin, K. Burke, *Physical Review A* **1995**, 51, 4531.
- [26] a) S. Wang, D. Fazzi, Y. Puttisong, M. J. Jafari, Z. Chen, T. Ederth, J. W. Andreasen, W. M. Chen, A. Facchetti, S. Fabiano, *Chem. Mat.* **2019**, 31, 3395; b) H. M. D. Michael Bendikov, Kyle Starkey, K. N. Houk, Emily A. Carter, and Fred Wudl, *J. AM. CHEM. SOC.* **2004**, 126, 7416.
- [27] T. K. S. Yamanaka, H. Nagao, K. Yamaguchi, *Chemical Physics Letters* **1994**, 231, 25.
- [28] G. Salvitti, F. Negri, A. J. Perez-Jimenez, E. San-Fabian, D. Casanova, J. C. Sancho-Garcia, *The journal of physical chemistry. A* **2020**, 124, 3590.
- [29] a) J. L. Bao, L. Gagliardi, D. G. Truhlar, *J Phys Chem Lett* **2018**, 9, 2353; b) C. M. Marian, A. Heil, M. Kleinschmidt, *WIREs Computational Molecular Science* **2018**, 9.
- [30] N. Dupuy, M. Casula, *The Journal of chemical physics* **2018**, 148, 134112.

- [31] D. Fazzi, E. V. Canesi, F. Negri, C. Bertarelli, C. Castiglioni, *Chemphyschem : a European journal of chemical physics and physical chemistry* **2010**, 11, 3685.
- [32] S. Canola, J. Casado, F. Negri, *Physical chemistry chemical physics : PCCP* **2018**, 20, 24227.
- [33] a) M. Casula, C. Attaccalite, S. Sorella, *The Journal of chemical physics* **2004**, 121, 7110; b) K. Nakano, C. Attaccalite, M. Barborini, L. Capriotti, M. Casula, E. Coccia, M. Dagrada, C. Genovese, Y. Luo, G. Mazzola, A. Zen, S. Sorella, *The Journal of chemical physics* **2020**, 152, 204121.
- [34] F. Plasser, H. Pašalić, M. H. Gerzabek, F. Libisch, R. Reiter, J. Burgdörfer, T. Müller, R. Shepard, H. Lischka, *Angewandte Chemie International Edition* **2013**, 52, 2581.
- [35] S. Grimme, A. Hansen, *Angewandte Chemie* **2015**, 54, 12308.
- [36] A. H. Christoph Alexander Bauer, and Stefan Grimme, *Chem. Eur. J.* **2017**, 23, 6150.
- [37] Y. D. Sofia Canola, Fabrizia Negri,, *Computation* **2019**, 7, 68.
- [38] a) I. H. Nayyar, E. R. Batista, S. Tretiak, A. Saxena, D. L. Smith, R. L. Martin, *Journal of Chemical Theory and Computation* **2013**, 9, 1144; b) C. R. M. Anderson, C. Fontanesi, A. Frick, S. Surana, D. Cheyys, M. Furno, T. Keller, S. Allard, U. Scherf, D. Beljonne, G. D'Avino, E. von Hauff, and E. Da Como, *Physica Review Materials* **2017**, 1, 9; c) D. Fazzi, M. Caironi, C. Castiglioni, *Journal of the American Chemical Society* **2011**, 133, 19056.
- [39] N. A. Deskins, M. Dupuis, *Physical Review B* **2007**, 75.
- [40] S. C. B. M. Alejandro L. Briseno, Patrick J. Shamberger, Fumio S. Ohuchi, Zhenan Bao, Samson A. Jenekhe, and Younan Xia, *Chem. Mat.* **2008**, 20, 8.
- [41] a) W. J. Kendrick, M. Jirásek, M. D. Peeks, G. M. Greetham, I. V. Sazanovich, P. M. Donaldson, M. Towrie, A. W. Parker, H. L. Anderson, *Chemical Science* **2020**, 11, 2112; b) S. Kahmann, D. Fazzi, G. J. Matt, W. Thiel, M. A. Loi, C. J. Brabec, *J Phys Chem Lett* **2016**, 7, 4438.